



A novel improved Harris Hawks optimization algorithm coupled with ELM for predicting permeability of tight carbonates

Navid Kardani¹ · Abidhan Bardhan² · Bishwajit Roy³ · Pijush Samui² · Majidreza Nazem¹ · Danial Jaled Armaghani⁴ · Annan Zhou¹

Received: 5 February 2021 / Accepted: 30 June 2021 / Published online: 26 July 2021
© The Author(s), under exclusive licence to Springer-Verlag London Ltd., part of Springer Nature 2021

Abstract

Tight carbonate reservoirs appear to be heterogeneous due to the patchy production of various diagenetic properties. Consequently, the permeability calculation of tight rocks is costly, and only a finite number of core plugs in any single reservoir can be estimated. Hence, in the present study, a novel hybrid model constructed by combination of the improved version of the Harris Hawks optimisation (HHO), i.e., IHHO, and extreme learning machine (ELM) is proposed to predict the permeability of tight carbonates using limited number of input variables. The proposed IHHO employs a mutation mechanism to avoid trapping in local optima by increasing the search capabilities. Subsequently, ELM-IHHO, a novel metaheuristic ELM-based algorithm, was developed to predict the permeability of tight carbonates. Experimental results show that the proposed ELM-IHHO attained the most accurate prediction with $R^2 = 0.9254$ and RMSE = 0.0619 in the testing phase. The result of the proposed model is significantly better than those obtained from other ELM-based hybrid models developed with particle swarm optimisation, genetic algorithm, and slime mould algorithm. The results also illustrate that the proposed ELM-IHHO model outperforms the other benchmark model, such as back-propagation neural nets, support vector regression, random forest, and group method of data handling in predicting the permeability of tight carbonates.

Keywords Permeability · Machine learning · Metaheuristic optimisation · HHO · IHHO · SMA

1 Introduction

To increase the efficiency of the production of hydrocarbon from unconventional reservoirs, the permeability of reservoir rocks should be measured with high accuracy [1]. The pulse decay technique can be used for an efficient

measurement of permeability in extremely tight rocks [2, 3]. This procedure tests the inlet pressure of a fixed mass of gas decreased when passing through a low-permeability sample. Nevertheless, this test may take several hours for extremely tight core plugs. To determine the Klinkenberg-corrected permeability coefficient, several measurements

✉ Navid Kardani
navid.kardani@rmit.edu.au

Annan Zhou
annan.zhou@rmit.edu.au

Abidhan Bardhan
abidhan@nitp.ac.in

Bishwajit Roy
bishwajit.roy@vitbhopal.ac.in

Pijush Samui
pijush@nitp.ac.in

Majidreza Nazem
Majidreza.nazem@rmit.edu.au

Danial Jaled Armaghani
danialarmaghani@susu.ru

¹ Civil and Infrastructure Engineering Discipline, School of Engineering, Royal Melbourne Institute of Technology (RMIT), Melbourne, VIC 3001, Australia

² Department of Civil Engineering, National Institute of Technology (NIT) Patna, Patna, Bihar 800005, India

³ School of Computing Science and Engineering, VIT Bhopal University, Bhopal, MP 466114, India

⁴ Department of Urban Planning, Engineering Networks and Systems, Institute of Architecture and Construction, South Ural State University, 76, Lenin Prospect, Chelyabinsk 454080, Russian Federation

should be made at different gas pressures [4]. Given that all tight rocks are vulnerable to gas slippage, the correction of gas slippage effects is extremely critical if precise permeability is possible [5]. These calculations are costly, and only a finite number of core plugs in any single reservoir can be estimated. Moreover, tight carbonate reservoirs appear to be heterogeneous due to the patchy production of various diagenetic properties [6, 7], which leads to modified petrophysical properties and quality of reservoirs at a range of scales. The permeability of heterogeneous tight carbonate reservoirs is usually not representatively calculated because an inevitably broad and costly procedure of achieving the appropriate dataset.

To mitigate the difficulties of laboratory experiments, different methods were presented to predict the permeability of the tight rocks expressed by k . In particular, via a mapping function where a set of rock properties is used as influential variables, the k value is calculated. Empirical equations attempting to equate k with rock properties, including the porosity, grain size, cementation factor, and etc., are the simplest ways of mapping functions. In the field of geotechnical engineering, the above empirical equations are commonly used to prevent rigours laboratory or field research. Nevertheless, because of the highly nonlinear stress-strain relationships, as well as elasto-plastic performance under loading and unloading conditions, these problems are highly complex. To adequately explain the mapping relationship between rock properties and k , conventional empirical equations are therefore inadequate. The main motivation of this study is to propose a simpler and more efficient way of determining the permeability of extremely tight, heterogeneous reservoir rocks which would help characterise these reservoirs as valuable and convenient technical resources.

In previous science and engineering investigations, machine learning algorithms (MLAs) have been employed as a predictive method [8–11]. This study does not aim to discuss MLAs and their application to address geophysical problems. The former has widely been studied, and the latter has been performed by skilful reviews. In the present study, we take into account some of the latest cases of ML applications to address geophysical and petrophysical problems. While several uses have been feasible, recent advancements include all aspects of logging petrophysics by determining facies and characterising rocks to define key criteria for measuring the reservoir's permeability and volumetrics. In logging, to dramatically boost the assessment of total organic carbon (TOC), the integrated hybrid neural network (IHNN) [12] and the integrated deep learning model (IDLM) [13] were introduced, allowing better characterisation of shale gas reservoirs. Onalo et al. [14, 15] used a nonlinear autoregressive network with exogenous inputs (NARX) to approximate the acoustic shear and compressional travel times in well logs and to find sufficiently detailed estimates

for actual sonic well logs. Most of the sonic properties like sonic porosity and Poisson's ratio could be predicted. ML was also employed for the calculation of the optimum reservoir characterisation parameters. Zhu et al. [16] latest study of water saturation in organic shale gas reservoirs, where genetic algorithms (GAs) are used to determine the shale petrophysical model's parameters, is a good example here. Electrical measurements as input are not required in this approach, so it is appropriate for organic shale reservoirs. Reservoir characterisation is also a multi-parametric problem that cannot be solved achieved. A hybrid GA-backpropagation neural network (BPNN) approach was demonstrated to be capable of forecasting fracture zones with shallow and deep electrical logs as input [17]. MLs have several advantages, including petrophysical characterisation and facies determination. To enhance the calculation of TOC, volatile hydrocarbons, and residual hydrocarbon, BPNNs and convolutional neural networks (CNNs) have been utilised [18], which outperforms the traditional approaches to the calculation of such parameters. Lim and Kim [19] introduced neural network and fuzzy logic approaches to estimate reservoir's permeability and porosity, showing the possibility for improvement in the future. Tang [20] and Tang et al. [21] employed probabilistic neural networks to categorise carbonate reservoirs facies with some success. Zhou et al. [22] sought to couple the diagenesis study and a deep autoencoder random forest algorithm to evaluate the relationship between the various conditions for diagnosis and the tight gas sandstone (TSG) reservoirs' electrical parameters (m and n values). Nevertheless, using a complex mixture of NMR data input and ML techniques, Zhu et al. [5, 23, 24] managed to reasonably predict TSG reservoir's permeability. Their findings were similar to those of Rashid et al. [25] using traditional permeability prediction methods.

Numerous researches have been carried out in science and engineering, to boost the performance of traditional MLAs, e.g., artificial neural network (ANN), adaptive neuro-fuzzy inference system (ANFIS), extreme learning machine (ELM), and so on [26–30]. As compared with statistical approaches, even if conventional MLAs achieve improved results, they are likely to be trapped into local minima instead of finding the precise global minimum, which generated unsatisfactory results. Therefore, to mitigate these problems, researchers currently use optimisation algorithms to update classical MLAs' learning parameters, yielding remarkable results [31–39]. This study utilises a recently developed metaheuristic optimisation algorithm, i.e., Harris Hawks optimization (HHO). Herein, a novel hybrid ELM-HHO approach is proposed, which is an integration of ELM and HHO algorithm. It may be noted that, ELM is a simple, fast, and an efficient ML algorithm, which shadows the structure of ANN. However, the working principle of ELM is somewhat different. With single layer of hidden neurons, ELM provides good generalisation performance at

extremely fast learning speed. HHO [40] is a recent MOA, which mimics Harris Hawk's actions in the search for and pursuit of rabbit in nature. It is a rapid, robust, and high-performance population-based MOA. It demonstrates better performance than other well-established algorithms (e.g., particle swarm optimization (PSO), GA, slime mould algorithm (SMA), etc.), yielding highly competitive outcome, based on experimental results from HHO authors. Therefore, HHO is employed herein to predict the permeability of tight carbonate reservoirs.

Nonetheless, like other MOAs, HHO has several shortcomings: (1) solutions are generated with limited diversity during the initialisation stage, (2) the problem of being caught up in the local minimum, (3) the problem of premature convergence, and (4) it is based on the rabbit energy starting at 2 and is concentrated gradually to 0 with the number of iterations. In the first half of the iterations, the algorithm completes the global search until the rabbit energy is larger than 1. This means that HHO does not carry out a global search procedure in the second half of the iterations. Premature convergence results in a local solution rather than a global solution. This research is, therefore, aimed at improving the standard HHO algorithm, depending on several factors. To circumvent the above problems and increase the performance of standard HHO algorithms, a mutation search method is integrated into the HHO algorithm. The improved HHO (IHHO) algorithm is subsequently utilised to develop an ELM-IHHO model to forecast the permeability of tight carbonates. Besides, a comparison is made between the proposed ELM-IHHO and ELM-HHO models and other well-established MOAs, e.g., PSO, GA, and SMA, integrated with ELM, including conventional back-propagation neural nets (BP-NN) [41], weighted ELM (WELM) [42], support vector regression (SVR) [43], random forest (RF) [44], and group method of data handling (GMDH) [45]. Successful application of these techniques can be found in [46–53]. It is important to mention that the successful applications of metaheuristic algorithms in increasing performance capacities of the base models, have been reported in literature [54–56]. This study also investigates the prediction capability of conventional regression model, i.e., multiple linear regression (MLR) for assessing the generalisation capability of the proposed ELM-IHHO model at all levels.

The remainder of this manuscript is structured into the following sections, including the introduction in the above section. Section 2 presents the Methodology of the study including the description of the models and hybridisation process, while Sect. 3 explains the detailed data processing and analysis, and performance parameters. This is followed by a detailed discussion on the performance of the developed soft computing models in the results and discussion in Sect. 4. Finally, advantages, limitations, and future scope of work Sect. 5, followed by summary and conclusions in Sect. 6 are presented.

2 Methodology and theoretical background of employed algorithms

2.1 Extreme learning machine (ELM)

ELM is a neural network-based model, novel data-driven tool that uses advanced single-hidden layer feed-forward neural network (SLFN) algorithm to provide a closed-form solution for the output weights using a least-squares solution. This is proceeded by fixing the weights and biases of the hidden layers. This model is extracted from a continuous probability distribution function instead of an iterative solution implemented by the traditional feed-forward ANN model. The great benefit of the ELM model lies in the smaller complexity involved in its architecture and its ability to overcome problems of regression (or classification) in a shorter time due to the randomisation of weights and biases of hidden neurons. Moreover, there is a specific least-square solution to the output, which can be solved using the Moore–Penrose inverse function. This eliminates the need for iterative models of training (e.g., ANN models) that appear to get caught up in local minima and not global minima, in a predictor dataset.

The ELM-based data modelling is a basic three-stage building process, carried out as follows: (1) randomly (not iteratively like ANN models) build up hidden layer weights and biases, (2) advance inputs through the parameters of the hidden layer to generate the output matrix of the hidden layer, and (3) evaluate output weights by the inversion of the output matrix of the hidden layer in which the Moore–Penrose's generalised inverse matrix is employed, followed by the calculation of its product with response variables (i.e., the solution to a set of equations) [57]. After identifying the nodes of the hidden neurons, this procedure entails randomising hidden neurons. A cross-validation dataset identifies hidden neurons using a trial-and-error approach. With greater foresight for real-time execution, ELM is superior over other models with data overfitting, slow convergence rates, inferior generalisation, iterative tuning, and local minima problems. Therefore, the swift and enhanced efficiency of ELM is beneficial in real-time applications.

An ELM model is used herein to train the target and predictor data pairs. Let x_i be the predictor and y_i be the target, for a group of d-dimensional vectors described for i ($i = 1, 2, \dots, N$) training samples, the SLFN with L hidden neurons can be expressed by

$$f_L(x) = \sum_{i=1}^L h_i(x)\beta_i = h(x) \beta, \quad (1)$$

where $\beta = [\beta_1, \beta_2, \dots, \beta_L]^T$ is the weight matrix of the output between the hidden and output neurons, $h(x) = [h_1, h_2, \dots, h_L]$ is the output of the hidden neurons representing the

randomised hidden features of the predictor x_i , and $h_i(x)$ is the i th hidden neuron. The hidden neuron output functions, $h_i(x)$, are represented as follows

$$h_i(x) = G(a_i, b_i, x), \quad a_i \in R^d, b_i \in R, \quad (2)$$

where $G(a_i, b_i, x)$ is a piecewise continuous nonlinear function which must satisfy the ELM approximation theorem. This function is defined by hidden neuron parameters (a, b). The sigmoid equation, commonly adopted in NN-based modelling, has been used in this study for developing the ELM model according to

$$\text{Log sigmoid} \Rightarrow G(a, b, x) = \frac{1}{1 + \exp(-ax + b)}. \quad (3)$$

When the weights linking the hidden layer and output layer (β) with the least square fitting are solved, the approximation error is to be minimised [58]:

$$\min_{\beta \in R^{L \times m}} H\beta - T^2,$$

where $\|H\beta - T\|$ is the Frobenius norm and H is the output matrix of the randomised matrix of the following form:

$$H = \begin{bmatrix} g(x_1) \\ \vdots \\ g(x_N) \end{bmatrix} = \begin{bmatrix} g_1(a_1x_1 + b_1) & \dots & g_L(a_Lx_1 + b_L) \\ \vdots & \ddots & \vdots \\ g_1(a_Nx_N + b_1) & \dots & g_L(a_Lx_N + b_L) \end{bmatrix}, \quad (4)$$

and the target matrix during data training can be expressed by

$$T = \begin{bmatrix} t_1^T \\ \vdots \\ t_N^T \end{bmatrix} = \begin{bmatrix} t_{11} & \dots & t_{1m} \\ \vdots & \ddots & \vdots \\ t_{N1} & \dots & t_{Nm} \end{bmatrix}. \quad (5)$$

Solving a system of linear equations yields an optimal solution

$$\beta^* = H^+T, \quad (6)$$

where H^+ is Moore–Penrose’s generalised inverse function (+). In Eq. (6), the optimum solution is used to determine a given input parameter x .

2.2 Theoretical background of MOAs

2.2.1 Harris Hawks optimisation (HHO)

HHO, a new optimisation approach developed by Heidari et al. [40], has been inspired by Harris Hawks birds’ behaviour in nature. It is based on the cooperation between the hawks in rabbit chasing and hunting. In HHO, a group of hawks tries to strike from different sides collaboratively while converging on a detected rabbit to hunt by surprise. Harris’s hawks demonstrate several chasing

tactics in different situations and the escaping strategies of the rabbit. When the team’s chief, i.e., the best hawk, strikes, and tracks the rabbit, it disappears suddenly from sight (vanishes into thin air). The next group member will continue with the chasing. This technique, i.e., switching tactic, leaves the rabbit fatigued and helpless and easily hunted. An advantage of the HHO algorithm is that it can be applied to constrained problems. It can also balance the exploration and exploitation phases and discovery as a global optimiser. The HHO algorithm consists of three major steps. The first step is the potential for exploration demonstrated by the following equation:

$$x(t+1) = \begin{cases} x_{\text{rand}}(t) - r_1|x_{\text{rand}}(t) - 2r_2x(t)| & q \geq 0.5 \\ x_{\text{rabbit}}(t) - x_m(t) - r_3(\text{LB} + r_4(\text{UB} - \text{LB})) & q < 0.5 \end{cases} \quad (7)$$

where $x(t)$ and $x(t+1)$ represent the hawk’s location in the current and next iterations, $x_{\text{rand}}(t)$ represents a randomly selected hawk from their current population, and $x_{\text{rabbit}}(t)$ represents the rabbit’s position. Additionally, r_1, r_2, r_3, r_4 , and q are randomly assigned numbers ranging from 0 to 1. LB and UB are lower and upper bounds, respectively. Moreover, x_m denote and the hawk’s average location, formulated as follows:

$$x_m(t) = \frac{1}{N} \sum_{i=1}^N x_i(t), \quad (8)$$

where $x_i(t)$ and N are each hawk’s position in t th iteration and the number of all hawks, respectively. The next is the transition phase between exploitation and exploration. The rabbit loses its energy continuously due to chasing and escaping. The following equation models the energy of the rabbit

$$E = 2E_0 \left(1 - \frac{t}{T}\right), \quad (9)$$

where E, E_0 , and T are rabbit’s escaping energy, rabbit’s initial energy, and the maximum number of iterations, respectively. In HHO, E_0 in any iteration can be altered randomly in the $[-1, 1]$ range. Therefore, exploitation and exploration occur when $|E| < 1$ and $|E| \geq 1$, respectively. The third step, i.e., exploitation, aims primarily to implement local solutions from previously established solutions. Here, hawks conduct the surprise attack to strike and detect the rabbit from the previous stage. According to the chasing tactic of hawks and escaping strategy of the rabbit, four methods were implemented to model the attacking stage:

1. *Soft besiege* It occurs when the rabbit has ample stamina, and hawks attempt to exhaust the rabbit. If r indicates the probability of effective escape, the strategy can be validated when $r \geq 0.5$ and $|E| \geq 0.5$. It can then be modelled by

$$x(t+1) = \Delta x(t) - E |Jx_{\text{prey}}(t) - 2x(t)|, \quad (10)$$

$$\Delta x(t) = x_{\text{prey}}(t) - x(t), \quad (11)$$

where $J = (1 - r_5)$ represents rabbit's jump strength, r_5 is a randomly assigned number ranging from 0 to 1, and $\Delta x(t)$ represents the difference between the rabbit's position and the rabbit's current position in the t th iteration.

2. Hard besiege This tactic is carried out when the rabbit lacks sufficient energy and is fatigued ($r \geq 0.5$ and $|E| < 0.5$). The updated positions can thus be defined by

$$x(t+1) = x_{\text{rabbit}}(t) - E_n |\Delta x(t)|. \quad (12)$$

3. Soft besiege with progressive rapid dive When $r < 0.5$ and $|E| \geq 0.5$, the rabbit still has enough energy to escape, and hawks make an intelligent move to determine their subsequent move, which is defined by

$$x = x_{\text{rabbit}}(t) - E |Jx_{\text{rabbit}}(t) - x(t)|, \quad (13)$$

$$Z = Y + S + \text{LF}(D), \quad (14)$$

where D , LF, and Z denote the dimension, Lévy flight function, and a $1 \times D$ random vector. Therefore, the positions of hawks are updated using the following model

$$x(t+1) = \begin{cases} Y & f(Y) < f(y(t)) \\ Z & f(Z) < f(y(t)) \end{cases}. \quad (15)$$

4. Hard besiege with progressive rapid dive When $r < 0.5$ and $|E| < 0.5$, this strategy is valid and can be modelled by

$$x(t+1) = \begin{cases} x_{\text{rabbit}}(t) - E |Jx_{\text{prey}}(t) - x_m(t)| & f(Y) < f(y(t)) \\ Z = Y + S + \text{LF}(D) & f(Z) < f(y(t)) \end{cases}. \quad (16)$$

2.2.2 Improved Harris Hawks optimisation (IHHO)

HHO is a robust and efficient metaheuristic algorithm for resolving real-world engineering problems. Nevertheless, based on the NFL (no free lunch) theorem, no algorithm is ideal for all optimisation problems [59]. Therefore, a mutation-based approach is implemented to develop the updated version of HHO, i.e., IHHO, to overcome HHO algorithms' shortcomings and boost its capacity for coping with real-world engineering problems. A mutation-based mechanism is employed to update each rabbit's current location by creating a diversified solution space for each iteration to improve the algorithm's local and global search capabilities. The velocity of the PSO can be used for this reason, which is given by

$$v_{m+1} = w \times v_m, \quad (17)$$

where w , v_m , and v_{m+1} denote the inertia weight, mutant velocity in the k th and $(k+1)$ th iteration. Each iteration uses Eq. (17) to update the mutant velocity. The updated velocity is then used to update the best rabbit's location by the following equation:

$$X_{\text{rabbit}} = X_{\text{rabbit}} + v_{m+1}. \quad (18)$$

The new position will be identified as a potential location if the new location's fitness is higher than the existing rabbit's location and will continue to boost the location by implementing the mutation strategy. The best location for the rabbits is then identified as a potential location for the rabbit. In the next iteration, the current and potential rabbit's locations are compared, and the optimum location is then selected. The steps of development of mutation-based IHHO algorithm is given in Fig. 1.

2.2.3 Particle swarm optimisation (PSO)

In 1995, Kennedy and Eberhart [60] introduced PSO as a member of the swarm-based metaheuristic group. Flocking and schooling patterns of birds and fish are the main source of inspiration for the PSO algorithm and finding globally optimal solutions in a multidimensional space is its main goal. As shown in Fig. 2, the PSO algorithm begins by initialising the random velocities and positions of the particles [61, 62]. Every particle then updates its location to identify the best position in the multidimensional space based on its velocity and personal best position as well as global best position. The best position achieved by individual particles is considered the global best position, whereas the best position obtained by the particle is considered the personal best location. The position of particle is updated according to its personal best position and the direction of the global best position. In the meantime, the particle velocities are updated on the basis of the difference between their personal best location and the global best location. The particles converge anywhere around the optimal solution using a mixture of exploitation and exploration.

$$V_i^{t+1} = \omega V_i^t + c_1 r_1^t (P_i^t - X_i^t) + c_2 r_2^t (P_g^t - X_i^t), \quad (19)$$

$$X_i^{t+1} = X_i^t + V_i^{t+1}. \quad (20)$$

In Eqs. (19) and (20), P represents position, V is velocity, g stands for global, i stands for personal and r_1 and r_2 are random numbers between 0 and 1. As trust parameters with a usual value of 2, c_1 and c_2 depend on the problem and show the confidence level of a particle against its personal

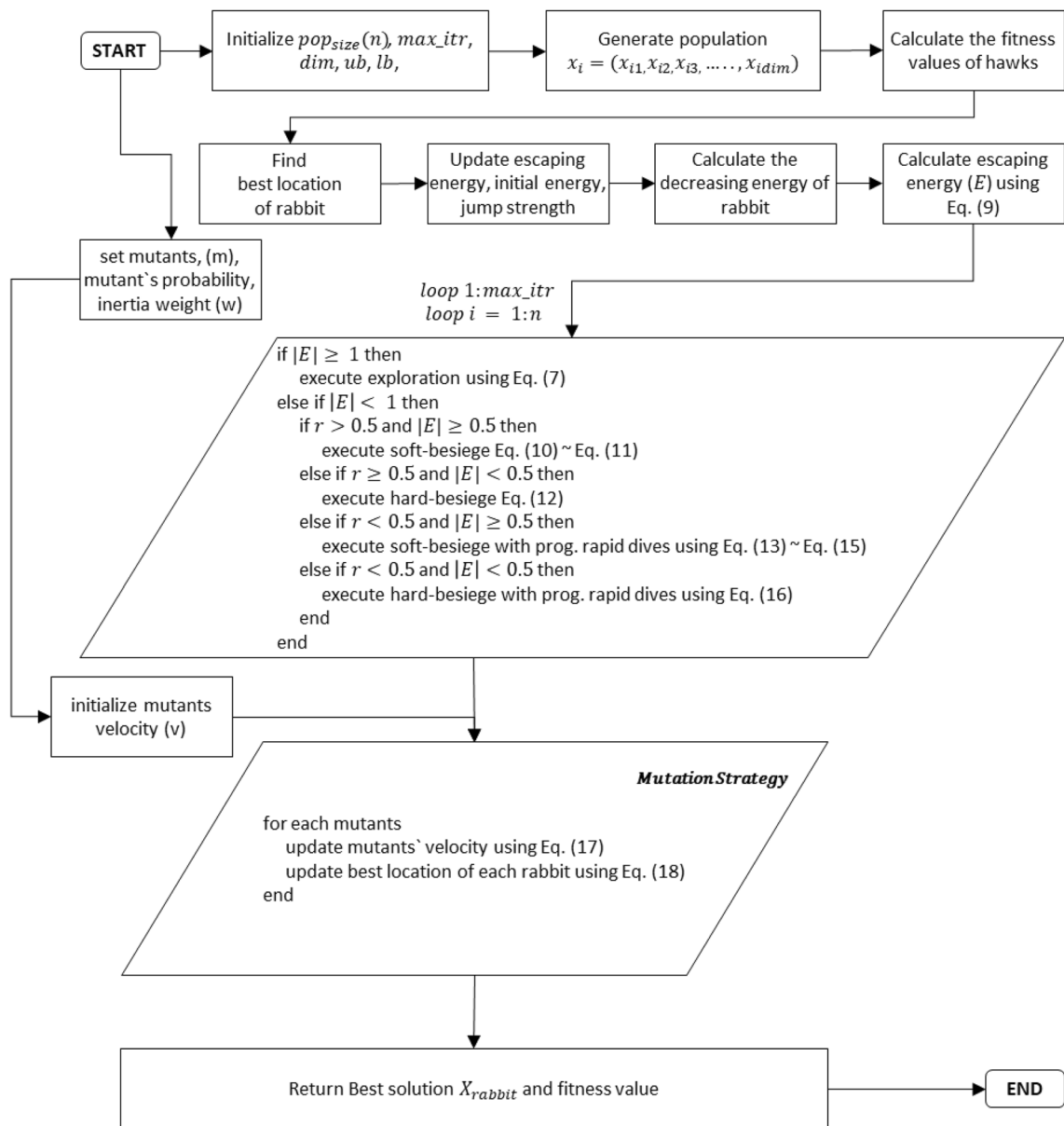
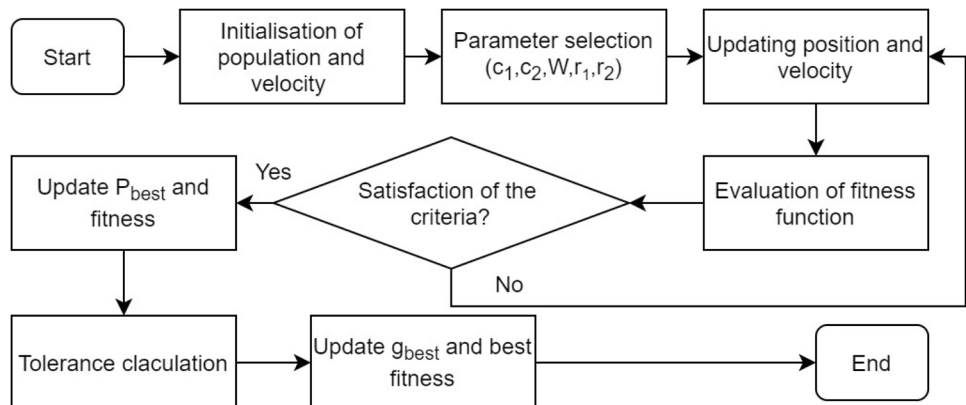


Fig. 1 Steps showing the development of IHHO algorithm

Fig. 2 Flow chart showing the steps of PSO algorithm



and global positions. Inertia weight is another parameter, represented by ω . Equation (21) shows the decreasing trend of inertia weight with time

$$\omega^t = \omega_{\max} - \frac{\omega_{\max} - \omega_{\min}}{t_{\max}} t. \quad (21)$$

In Eq. (21), primary and final inertia weights are, respectively, shown by ω_{\min} and ω_{\max} with recommended values of 0.4 and 0.9, and t_{\max} depends on the maximum number of iterations. Genetic algorithm (GA) resembles PSO in many ways; however, particles support one another in the PSO algorithm in contrast to their competition in GA. As the main characteristic of PSO, its large number of particles makes it distinct from other optimisation approaches and allows for finding globally optimal solutions.

2.2.4 Genetic algorithm (GA)

The GA, first introduced by Holland [63], is a mathematical representation of human biological and natural evolution. GA has been implemented for numerous applications to generate satisfactory results. In GA, the best responses of a certain generation are paired to obtain the optimum solution, based on the theory of survival of the fittest. Chromosomes are selected randomly from the current populations (parents) and generate the next generation in each stage. For this reason, three major genetic operators are employed in each stage, i.e., selection operator, crossover operator, and mutation operator.

The selection operator chooses a member in a generation to take part in the reproduction process based on fitness criteria. Chromosomes with a better fit are likely to be selected. The crossover operator seeks to generate offspring by randomly choosing a locus between two chromosomes. Crossover contributes to the random generation of new solutions based on the current population. The crossover point is chosen randomly in the range 1 and $\min(LA^{P_1}, LA^{P_2}) - 1$, where LA^{P_1} and LA^{P_2} are the number of position areas for P_1 and P_2 parent solutions. The mutation operator re-permutes the chromosomal bit sequence randomly such that the topology is not altered, but creates different placements.

Step 1 Initialise potential problem solutions (random chromosome n population).

Step 2 Determine the population's fitness for each chromosome.

Step 3 Complete these steps to create n offspring and execute them.

Choose a chromosome pair correlated with the role of the parents. Individuals are selected probably based on fitness criteria.

The pair can be crossed at a randomly selected location due to the probability of two generations. If no crossover

occurs, establish two heirs who are exact copies of their ancestors. The mutation of the two generations (the rate of change) on any locus may occur according to the probability. Therefore, the new generation should place the resulting chromosomes.

Step 4 Replace the existing population with the new population.

Step 5 If the stop conditions are not fulfilled, go to Step 2 or have the best solution.

Figure 3 shows the entire process of GA in the form of flowchart.

2.2.5 Slime mould algorithm (SMA)

The function and morphological variations of slime mould *Physarum polycephalum* in foraging are affected by the slime mould algorithm [64]. This algorithm does not represent a full life cycle. The positive and negative feedback caused by slime mould throughout foraging, however, are aroused by the application of weights in SMA. Hence, a new idea of a brand is to shape three diverse morphotypes. Cold and humid places are optimum conditions for slime mould (eukaryote). Plasmodium is the preliminary nutritional stage, which is dynamic, active, and the first research step of the algorithm. Exploring, encompassing, and secreting enzymes to absorb the food, by the natural material in slime mould occur in this step. The leading end, during the immigration procedure, is shaped like a fan. As a result, an interconnected venous system happens and leads to the internal flow of the cytoplasm. They have a different pattern and property; hence it helps them to utilise various food sources to shape a pairing venous network. The growth of the slime mould to more than 900 square centimetres depends on the food supply in the environment. The bio-oscillator, after which a vein attains a food supply, provides an increasing wave to improve the cytoplasmic flow through the vein. The rate of the cytoplasm flows holds a negative relationship with the density of the vessel. Here, with both positive and negative feedbacks, slim provides the optimal way; hence it can combine food in a relatively superior way. So, we have a numerically represented slime mould and used it with diagram story and pathway networks. Here are the main steps representing the numerical example of slime:

1. Phase of approach food

The odour circulating in the air directs the slime mould to surround the food. Following equation mimics, the compression mode, which manifests its rising behaviour in the numerical method

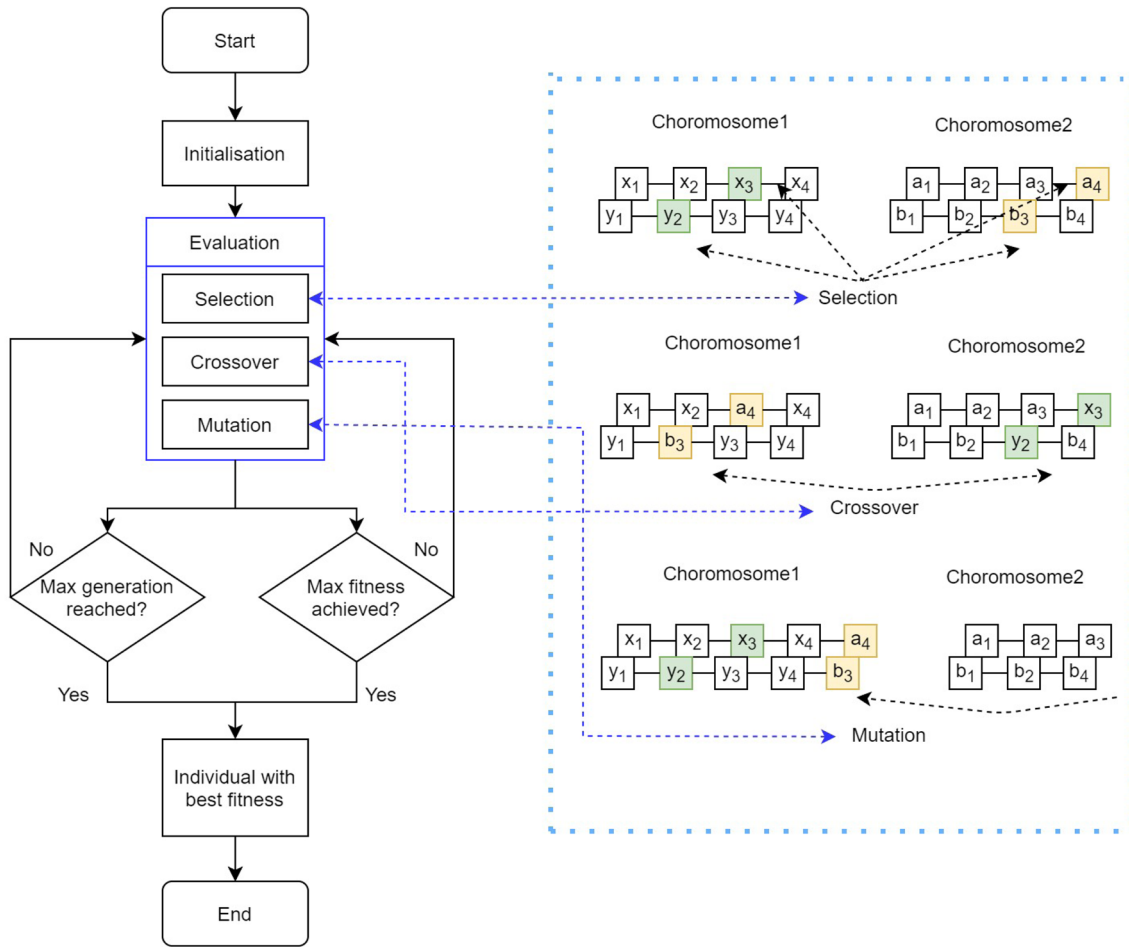


Fig. 3 Flow chart showing the steps of GA

$$X(\vec{t} + 1) = \begin{cases} \vec{X}_b(t) + \vec{v}b \cdot (\vec{W} \cdot \vec{X}_A(t) - \vec{X}_B(t)), & r < p \\ \vec{v}c \cdot \vec{X}(t), & r \geq p \end{cases}, \quad (22)$$

where $\vec{v}b$ ranges between $[-a, a]$, $\vec{v}c$ reduces linearly in the range of one to zero, t stands for the current iteration, \vec{X}_b represents the personal place with the maximum odour density ever found, \vec{X} shows the place of slime mould, \vec{X}_A and \vec{X}_B are two individuals randomly chosen from slime mould, \vec{W} shows the rate of slime mould, and p is obtained by

$$p = \tanh|S(i) - DF|, \quad (23)$$

in which $i \in [1, 2, \dots, n]$, $S(i)$ shows the accuracy of \vec{X} , DF shows the optimal fitness in all repetitions. Vector $\vec{v}b$ is calculated by

$$\vec{v}b = [-a, a], \quad (24)$$

$$a = \text{arc tanh}\left(-\left(\frac{t}{\max - t}\right) + 1\right), \quad (25)$$

\vec{W} is computed by

$$W(\text{Smell Index}(i)) = \begin{cases} 1 + r \cdot \log\left(\frac{bF - S(i)}{bF - wF} + 1\right), & \text{condition} \\ 1 - r \cdot \log\left(\frac{bF - S(i)}{bF - wF} + 1\right), & \text{others} \end{cases}, \quad (26)$$

$$\text{Smell Index} = \text{sort}(S). \quad (27)$$

$S(i)$ places the first share of the state. The casual amount in the period of $[0, 1]$ is shown by r . $\max - t$ stands for the highest iteration. The optimal adaptation achieved in the casual iterative manner is shown by bF , the worst adaptation amount received in the iterative method currently represented by wF . Smell Index expresses the order of fitness values sorted. Based on the most suitable location \vec{X}_b , individual \vec{X} is updated, and the fine-tuning of parameters $\vec{v}b$, $\vec{v}c$ and \vec{W} are changing the location of the individual. Individuals can also make search vectors at all angles, i.e., solution space in any directions, so this algorithm will potentially attain the best resolution. As shown in Eq. (22), individuals

can search in all reasonable directions close to the optimal solution; hence, while approaching the food, they affect the circular sector construction of a slime mould. This concept can be generalised to a hyper-dimensional space.

2. Phase of wrap food

While searching, this part is simulating the contraction mode of venous tissue structure of slime mould mathematically. The concentration of food contacted by the vein has a positive relationship with the power of the wave that is generated by the bio-oscillator, the rate of cytoplasm flows, and the concentration of the vein. The positive and negative feedbacks between the vein width of the slime mould and the food concentration, as shown in Eq. (26), is mathematically simulated. The possibility of venous compression mode is simulated by r (Eq. 26). The rate of the statistical value is reduced by log, but the amount of compression frequency shifts slightly. After affecting the slime mould by condition, its search models will adapt based on food quality. The weight near the region depends on the food supply, less food concentration, less rate of the region; hence leads to the exploration of other regions. So, the resulting formula is as follows

$$\vec{X}^* = \begin{cases} \text{rand} \cdot (\text{UB} - \text{LB}) + \text{LB}, & \text{rand} < z \\ \vec{X}_b(t) + \vec{v}b \cdot (\vec{W} \cdot \vec{X}_A(t) - \vec{X}_B(t)), & r < p \\ \vec{v}c \cdot \vec{X}(t), & r \geq p \end{cases} \quad (28)$$

where LB and UB show the lower and upper restrictions of the search area, rand and r show the random amount in $[0,1]$, the value of z will be presented in the parameter setting analysis.

3. Phase of oscillation

The cytoplasmic flow in veins will be modified based on the slime mould, which is generated by the biological oscillator. Hence, they provide a more convenient statue of the food supply. Managing \vec{W} , $\vec{v}b$ and $\vec{v}c$ to understand the variations will mimic the diversity of venous amplitude of slime mould. The oscillation frequency of the slime mould was mathematically simulated using \vec{W} near one at different food concentrations in a way that the slime mould more quickly approached a high-quality food and more slowly as the food concentration was lower in the individual's location, thus enhancing the efficiency of the slime mould in selecting the food source. The amount of $\vec{v}b$ ranges between $[-a, a]$ and gradually approached 0 with the number of iterations. $[-1, 1]$ shows the range of $\vec{v}c$, and at last, this amount approaches zero. The particular function of slime mould has followed by the synergistic interplay between $\vec{v}b$ and $\vec{v}c$. Generally, to

find a more reliable origin of food, it will still depart some organic material for investigating other areas in an endeavour to find a more leading quality source of food, rather than investing all of it in one source.

The position of slime mould, however, is aroused by the oscillation method of $\vec{v}b$. It determines progressing the food origin or obtaining other food origins. Note that it is not easy to probe food. Many factors may restrict this period, such as light and dry environment, binding the spread of slime mould. As a result, the probability of slime mould to discover more leading quality food will increase, which results in avoiding the trapping of regional maximum.

2.3 Hybridisation process

Several studies were conducted in engineering applications to increase the efficiency of classical ML models such as ANN, ANFIS, SVM, and LSSVM, by incorporating MOAs [65–67]. Many real-time data often do not conform to particular laws or distributions but are typically nonlinear with mixed noise. Therefore, real-time data are difficult to handle to develop a predictive model using conventional ML methods. The inability to find the exact global minimum, in particular, affects the efficiency of conventional ML models, yielding unsatisfactory results and giving rise to overfitting problems in the estimation of a new data set. The ANN's local minima trapping problem often results in inaccurate results. Hence, to circumvent these obstacles, scholars use hybrid models to find the exact global minimum instead of the local minimum, through updating learning parameters, i.e., W&B (weights and biases) of binding neurons via the integration of MOAs [68, 69] with conventional ML models (e.g., ANN, ANFIS, LSSVM and SVM).

ELM involves the random initialisation of learning parameters (e.g., input-to-hidden-layer weights and hidden-to-output layer W&B of hidden neurons), potentially yielding unsatisfactory and inefficient ELM's performance due to local minima trapping problem. Therefore, to minimise this problem, MOAs can be incorporated to find the exact global minimum and optimal W&B. In this study we employ the recently developed HHO algorithm to optimise ELM's learning parameters. The ELM-HHO includes following steps:

- Start with parameter setting (e.g., hidden neuron number) and random W&B generation at the initial level,
- Produce optimal W&B by HHO, and
- Finally, the model is validated by HHO's optimal W&B.

For other MOAs, the same process was followed to produce optimal W&B.

However, in the "Results and discussion" section, the details of the parametric configuration of the MOAs (e.g.,

HHO, IHHO, PSO, GA and SMA) are presented. Figure 4 demonstrates the hybridisation process herein and the steps to develop the metaheuristic models coupled with ELM.

3 Data and metrics

3.1 Data preparation

In this study, 130 cases of tight carbonates are collected from experiments [70, 71] to form the main dataset. The core plugs were derived from the Portland Formation in the southern England at $50^{\circ} 33' 10''$ N $02^{\circ} 26' 25''$ W. This study aims to predict the permeability of tight carbonates using the limited number of influential variables which are attained cheaply, easily and routinely from the typical core plug measurements. To achieve this aim, three properties including porosity ϕ , formation resistivity factor F , and pore throat diameter D_{pt} (m) are considered as the input variables, while the permeability k (mD) is the output variable. Helium porosity method was selected to measure ϕ as the water saturation porosity method could not be considered due to the physical nature of the tight carbonates. In addition, mercury injection capillary pressure measurements and fluid permeability method were also employed for each case to determine the associated variable. Table 1 shows the core plug properties used in this study, while Fig. 5 shows the linear relationships between the variables as well as their distributions.

3.2 Data processing and performance metrics

Five FLM-coupled metaheuristic models have been developed and suggested in this research. These include ELM-HHO, ELM-IHHO, ELM-PSO, ELM-GA, and ELM-SMA. The ‘min–max’ technique is employed to normalise the

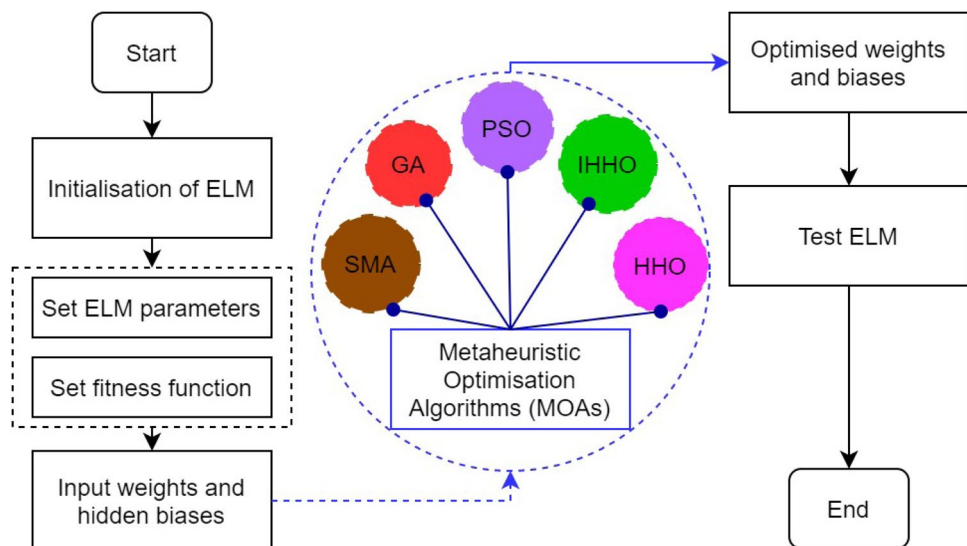
Table 1 Statistical summary of the input and output variables

	ϕ (–)	F (–)	D_{pt} (m)	k (mD)
Mean	0.1790	62.2692	2.8844e–08	0.005244
Standard deviation	0.0370	29.5644	4.0637e–08	0.020163
Minimum	0.1070	17.0000	3.9200e–10	0.000002
1st quartile	0.1512	40.0000	6.5800e–09	0.000032
2nd quartile	0.1730	55.0000	1.3650e–08	0.000213
3rd quartile	0.2150	74.7500	3.2500e–08	0.001227
Maximum	0.2650	200.0000	2.2800e–07	0.185000

whole dataset. The most important step in soft computing is data normalisation, a pre-processing task in every problem. Data normalisation is usually carried out to nullify the variables’ dimensional effects. Hence, the ‘min–max’ normalisation technique is employed during pre-processing for data normalisation within a specified range of upper bound 1 and lower bound 0. The dataset was eventually split into two subsets, namely training subset and testing subset. In this respect, 75% (i.e., 98 observations) of the main dataset is randomly extracted to create the training subset, while the remaining 25% (32 observations) is used as the testing subset. The next move is to use the training dataset to train the proposed models and the testing dataset to validate them. Figure 6 illustrates the entire process, including data collection, normalisation and partitioning, processing and developing computational models, and predicting the output.

The next step involves determining and comparing 10 performance indices in every possible way to examine the performance of developed models [31, 72–75]. These include coefficient of determination (R^2), Legate and McCabe’s Index (LMI), Willmott’s Index of agreement (WI), variance account factor (VAF), NS, root mean square error (RMSE), mean absolute error (MAE), mean bias error (MBE), root mean

Fig. 4 Hybridisation process of the ELM-based MOA models



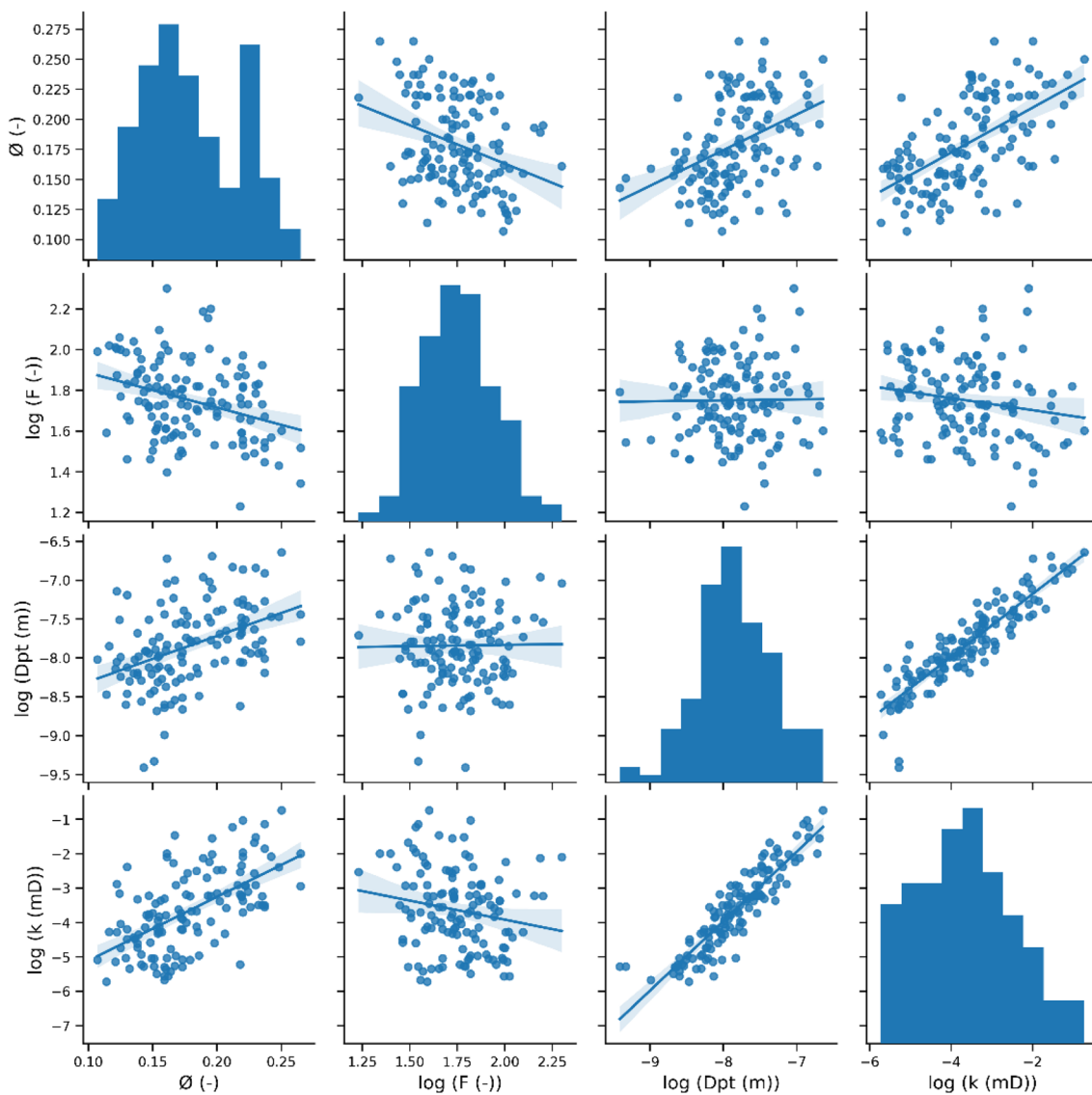


Fig. 5 Scatter plots of the variables against each other along with their distributions

square error to observation's standard deviation ratio (RSR) and weighted mean absolute percentage error (WMAPE). The motive behind the use of different performance parameters was to evaluate the performance of the prediction models from different aspects, such as associated error, degree of correlation, and variance in error between the observed and predicted values. These indices are defined by:

$$R^2 = \frac{\sum_{i=1}^n (y_i - \bar{y})^2 - \sum_{i=1}^n (\hat{y}_i - \bar{y})^2}{\sum_{i=1}^n (y_i - \bar{y})^2}, \quad (29)$$

$$LMI = 1 - \left[\frac{\sum_{i=1}^n |y_i - \hat{y}_i|}{\sum_{i=1}^n |y_i - \bar{y}|} \right], \quad (30)$$

$$WI = 1 - \left[\frac{\sum_{i=1}^n (y_i - \hat{y}_i)^2}{\sum_{i=1}^n \{|\hat{y}_i - \bar{y}| + |y_i - \bar{y}|\}^2} \right], \quad (31)$$

$$VAF (\%) = \left(1 - \frac{\text{var}(y_i - \hat{y}_i)}{\text{var}(y_i)} \right) \times 100, \quad (32)$$

$$NS = 1 - \frac{\sum_{i=1}^n (y_i - \hat{y}_i)^2}{\sum_{i=1}^n (y_i - \bar{y})^2}, \quad (33)$$

$$RMSE = \sqrt{\frac{1}{n} \sum_{i=1}^n (y_i - \hat{y}_i)^2}, \quad (34)$$

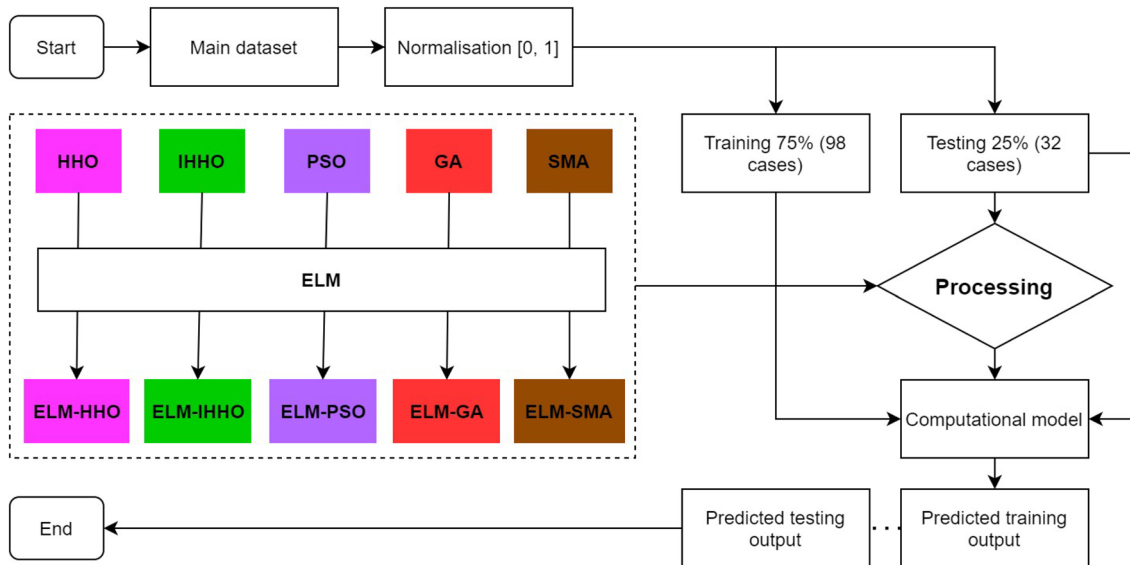


Fig. 6 Flow chart showing the methodology of this study

$$\text{MAE} = \frac{1}{n} \sum_{i=1}^n |(\hat{y}_i - y_i)|, \quad (35)$$

$$\text{MBE} = \frac{1}{n} \sum_{i=1}^n (\hat{y}_i - y_i), \quad (36)$$

$$\text{RSR} = \frac{\text{RMSE}}{\sqrt{\frac{1}{n} \sum_{i=1}^n (y_i - \bar{y}_{\text{mean}})^2}}, \quad (37)$$

$$\text{WMAPE} = \frac{\sum_{i=1}^n \left| \frac{y_i - \hat{y}_i}{y_i} \right| \times y_i}{\sum_{i=1}^n y_i}, \quad (38)$$

where n denotes the number of observations for the corresponding parameters, y_i and \hat{y}_i represent the real desired output's actual and modelled value i , i.e., permeability. Additionally, \bar{y}_{mean} represents the average of input variables. The optimal values of these indices are presented in Table 2.

4 Results and discussion

This section summarises the results of the developed models for estimating the permeability of tight carbonates using three rock characteristics (i.e., ϕ , F , and D_{pt}). The models are developed and validated using the training dataset (98 observations) and the testing dataset (32 observations). The results of all models are presented as follows.

Table 2 Ideal values of performance indices

Trend indices	Ideal value	Error indices	Ideal value
R^2	1	RMSE	0
LMI	1	MAE	0
WI	1	MBE	0
VAF	100	RSR	0
NS	1	WMAPE	0

4.1 Model implementation

The parametric configurations and their optimal values are demonstrated in Table 3. As previously stated, the deterministic parameters of MOAs and the number of hidden neurons of ELM must be tuned to create the optimal hybrid model. This study investigates the number of hidden neurons (i.e., 5–20) in each run to optimise the W&B of the attaching neurons. The optimal number of hidden neurons was obtained to be 15 following a primary trial-and-error run. In the course of simulations, several deterministic parameters are tuned. These include the cognitive coefficient (C_1) and social coefficient (C_2), inertia weights (w_{\max}, w_{\min}), size of the particle swarm population (n), the maximum number of iterations (t), and other MOA parameters. Table 3 demonstrates the optimum values of these parameters w .

Once ELM-based metaheuristic models are trained, their final configuration is finalised. In the modelling based on the ELM, there are 150 ($15 \times 9 + 15$) optimised learning parameters. The optimal number of hidden neurons reached in the ELM-HHO model was used and held constant during this study to contrast the proposed models fairly. However, the

Table 3 Parameter configuration of the hybrid models

Parameters	ELM-HHO	ELM-IHHO	ELM-PSO	ELM-GA	ELM-SMA
Number of hidden neurons in ELM (N)	15	15	15	15	15
Maximum number of Iterations (t)	500	500	500	500	500
Particle/swarm/population size (n)	25	25	25	25	25
Lower bound, upper bound	−1, +1	−1, +1	−1, +1	−1, +1	−1, +1
Cognitive coefficient (C_1), social coefficient (C_2)	—	—	1, 2	—	—
Inertia weights (w_{\max}, w_{\min})	—	—	0.90, 0.40	—	—
Inertia weights (w)	—	0.40	—	—	—
Mutation probability	—	0.01	—	0.01	—
Mutants' percentage	—	0.90	—	—	—
β	—	—	—	1.00	—
γ	—	—	—	0.80	—
z	—	—	—	—	1.00
Cost/fitness function	RMSE	RMSE	RMSE	RMSE	RMSE

procedures of ELM-HHO, ELM-IHHO, ELM-PSO, ELM-GA, and ELM-SMA are explained in the following.

The ELM is initialised first in ELM-HHO modelling. Afterwards, the HHO algorithm is utilised for optimising the W&B of ELM to determine the permeability of tight carbonates. RMSE is exploited as a fitness function in any iteration during optimisation. The search operation is conducted in 100–500 iterations with $n=10$ –25 to ensure that the W&B and other parameters of chosen ELM-HHO model are optimised. Finally, the ELM-HHO model with optimal deterministic parameter values obtained in the trial-and-error run can be characterised as follows: the number of hidden neurons (N) = 15, population size (n) = 25, and the maximum number of iterations (t) = 500. Optimal W&B values of attaching neurons are then employed to estimate the new dataset, namely the testing dataset. The predictive performance of ELM-HHO model is illustrated in Figs. 7 and 8, respectively, for the training dataset and testing dataset.

As with the ELM-HHO model, a mutation-based HHO algorithm (i.e., IHHO) is utilised to optimise the W&B of ELM after ELM initialisation. The ELM-IHHO model is trained with the same optimal value for HHO parameters. The IHHO algorithm's mutation parameters are therefore set as follows: inertia weight (w) = 0.80, mutation rate = 0.05, mutation probability = 0.001, including the hidden neurons (N) = 15, population size (n) = 25, and maximum number of iterations (t) = 500. The binding neurons' optimal W&B values are then employed to predict a new data set. In ELM-IHHO modelling, the mutation-based mechanism is implemented integrated into the standard HHO algorithm to improve the efficiency of the ELM-HHO model. Figures 6 and 7, respectively, demonstrate the results of k prediction during the training and testing phases. While the number of input and hidden

neurons and iterations and population size are identical, optimal W&B values of ELM-IHHO models are different.

The same procedure is followed to optimise W&B of ELM using PSO, GA, and SMA, as they have been implemented in ELM-HHO and ELM-IHHO modelling. In this respect, the trial-and-error approach is utilised to tune the PSO, GA, and SMA parameters to provide the best predictive ELM-PSO, ELM-GA, and ELM-SMA models for each scenario. The maximum number of iterations (t) and the swarm particle size (n) are held constant in all situations. In PSO, cognitive coefficient (C_1) = 1, social coefficient (C_2) = 2, $w_{\max} = 0.90$; and $w_{\min} = 0.40$, in GA, mutation probability = 0.01, $\gamma = 0.80$ and $\beta = 0.50$, and in SMA, $z = 1$. These parameters need to be set before ELM optimisation. Finally, the least possible RMSE determines the optimum ELM-PSO, ELM-GA, and ELM-SMA models with ideal W&B values. Figures 7 and 8 display the prediction results of the training dataset and testing dataset, respectively. Herein, the prediction results of the developed hybrid models are shown.

Looking at the bar plot depicted in Fig. 9f, the efficacy of the proposed ELM-IHHO model can be evaluated, where the computation time of all algorithms is presented graphically. The computation time is estimated to be 34.1971, 80.2011, 31.1410, 31.7651, and 36.0081 secs for HHO, IHHO, PSO, GA, and SMA, respectively, after 500 iterations. According to the results, comparing IHHO and HHO revealed that the former had a computation time of 60.91% less than the latter. Also, a combined iterative performance is given in Fig. 9g for easy comparison. This renders IHHO a robust and efficient algorithm compared to HHO and other algorithms proposed here.

Moreover, the convergence behaviour of MOAs plays a crucial role in assessing their performance. Convergence demonstrates the probability of escaping local optima by

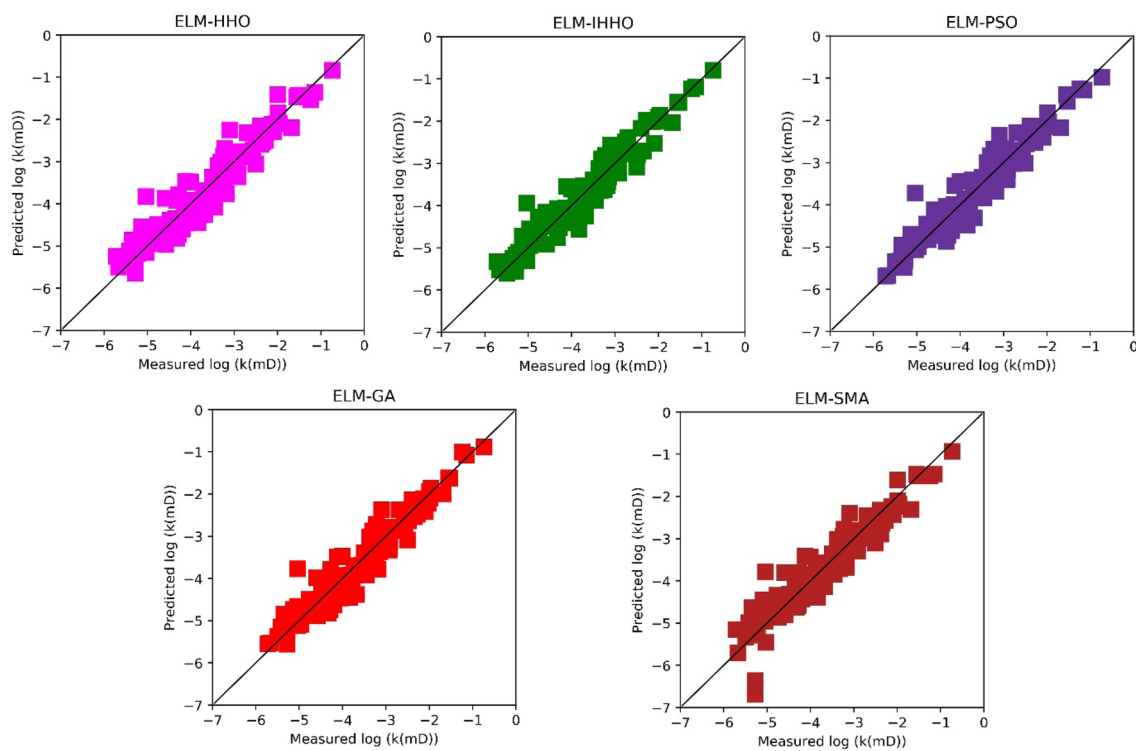


Fig. 7 Regression plots between measured and predicted values for ELM-based hybrid models at the training stage

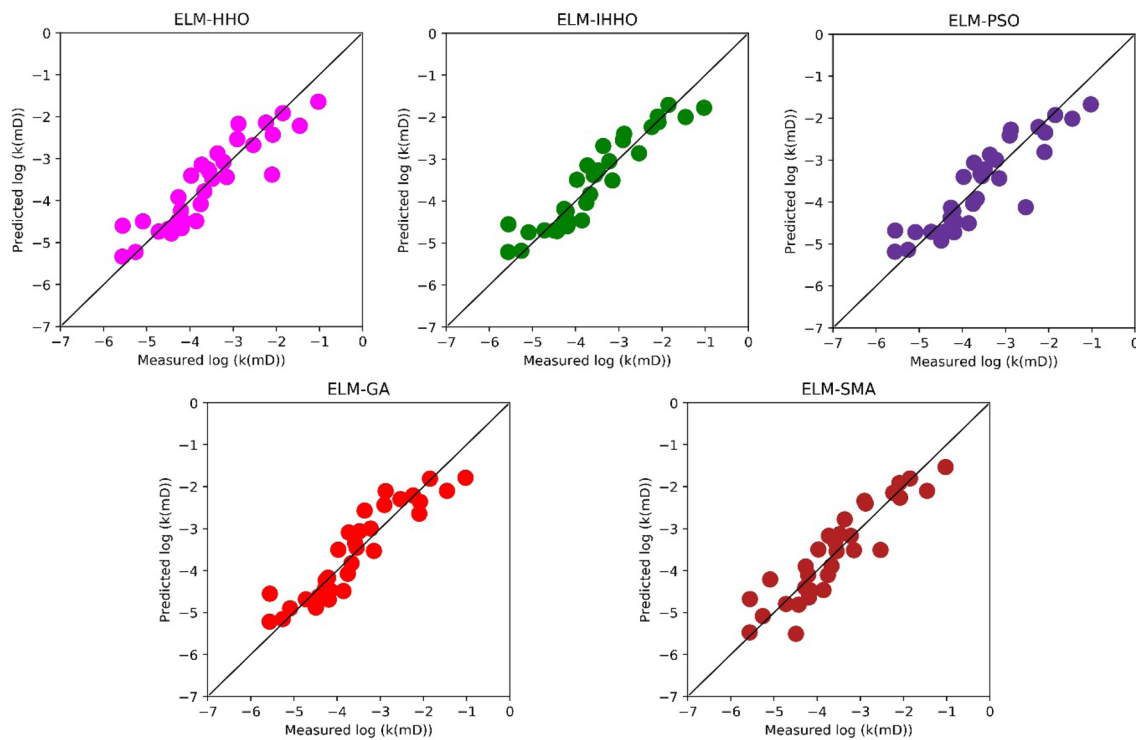


Fig. 8 Regression plots between measured and predicted values for ELM-based hybrid models at the testing stage

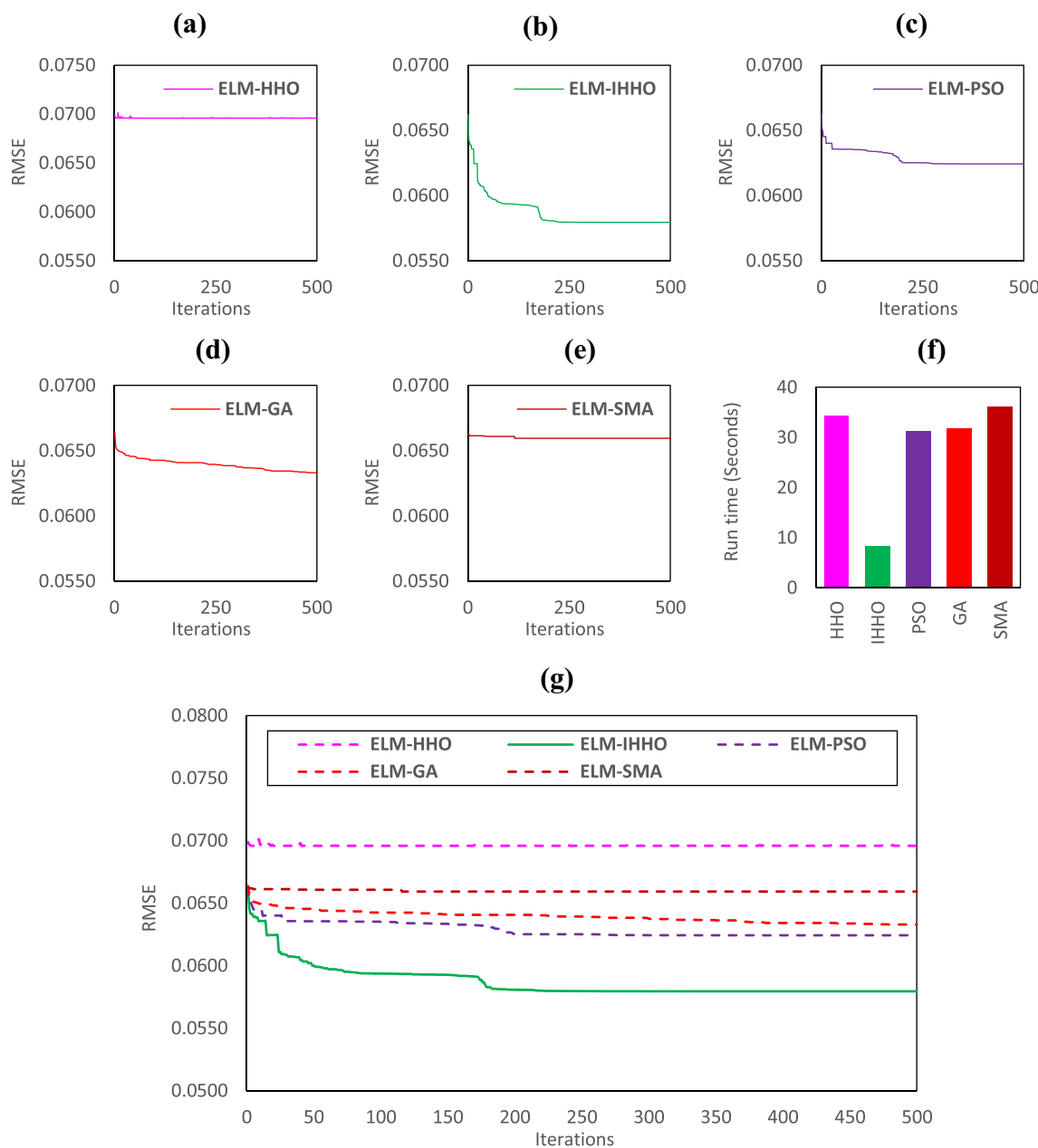


Fig. 9 Convergence curve and iterative performance of the proposed hybrid models in order as **a–e** model wise convergence curve; **f** computational time in s; and **g** convergence curve of all model in a single graph

the optimisation algorithm. Algorithms with exploration-exploitation dilemma are more likely to get trapped in local optima. Figure 9a–e provide a comparison of ELM-IHHO convergence with other algorithms, such as ELM-HHP, ELM-PSO, ELM-GA, and ELM-BBO. The convergence curves reveal that the IHHO algorithm is quicker than ELM-based MOA in finding the superior solution, suggesting that the IHHO algorithm is superior in ELM-IHHO modelling.

4.2 Statistical details of the results

In this section, to have a better insight to the efficiency of the proposed hybrid model, five well-known conventional ML models, namely WELM, BP-NN, SVR, RF, and GMDH are analysed and compared. MLR, as a base line model, is also applied to the dataset in the training and testing stages and the obtained results are compared to the ones from proposed hybrid models in different ways.

Once models are developed, the generalisation capability and efficiency will be evaluated using several performance indices mentioned in Sect. 3.2. To achieve this, the values of 10 performance indices (R^2 , LMI, WI, VAF, NS, RMSE, MAE, MBE, RSR, and WMAPE) for each of the five models are individually evaluated, as shown in Tables 4 and 5 for training as well as testing data sets. It is observed that all models are able to mimic the relationships in predicting the k . As suggested, the five of the six proposed hybrid models obtained an R^2 value of over 90% accuracy during the training phase. The values of R^2 above 0.90 suggest that the models have obtained an excellent fit to the experimental results. According to the statistical results derived from R^2 , RMSE, and MEA metrics, in the training stage, ELM-IHHO shows the best predictive performance with $R^2 = 0.9394$, RMSE = 0.0580 and MAE = 0.0451. This is followed by ELM-PSO with $R^2 = 0.9297$, RMSE = 0.0625 and MAE = 0.0467, ELM-GA with $R^2 = 0.9277$, RMSE = 0.0633 and MAE = 0.0480, and ELM-HHO with $R^2 = 0.9126$, RMSE = 0.0696 and MAE = 0.0546. In addition, ELM-SMA with $R^2 = 0.8847$, RMSE = 0.0800 and MAE = 0.0617 is identified as the weakest amongst hybrid models. Furthermore, BP-NN

shows the best predictive performance amongst the conventional models with $R^2 = 0.9159$, RMSE = 0.0683 and MAE = 0.0537, which is the only conventional model with R^2 value of over 90%. This is followed by GMDH, SVR, MLR, RF, and WELM. For the testing stage, the best predictive performance is achieved by ELM-IHHO, same as the training dataset, with $R^2 = 0.9254$, RMSE = 0.0619 and MAE = 0.0485, and ELM-PSO stands as the second-best model in the testing stage with $R^2 = 0.9176$, RMSE = 0.0652 and MAE = 0.0519. ELM-IHHO and ELM-PSO are followed by ELM-HHO with $R^2 = 0.9042$, RMSE = 0.0712 and MAE = 0.0482, ELM-GA and ELM-SMA with $R^2 = 0.8840$, RMSE = 0.0776 and MAE = 0.0620 and $R^2 = 0.8265$, RMSE = 0.0955 and MAE = 0.0777, respectively. For the conventional models, it should be noted that all the R^2 values are below 90% at the testing stage, while BP-NN shows the best performance with $R^2 = 0.8933$, RMSE = 0.0742 and MAE = 0.0617. These results suggest that strong predictive performance has been achieved by the proposed metaheuristic ELM-based models. Other indices show good predictive accuracy. Tables 4 and 5 depict the detailed summary of the

Table 4 Values of performance indices of the hybrid models for the training stage

Indices	ELM-HHO	ELM-IHHO	ELM-PSO	ELM-GA	ELM-SMA	WELM	BP-NN	SVR	RF	GMDH	MLR
R^2	0.9126	0.9394	0.9297	0.9277	0.8847	0.6848	0.9159	0.8940	0.8095	0.8943	0.8847
LMI	0.7216	0.7699	0.7621	0.7552	0.6854	0.2094	0.7265	0.0690	0.5539	0.6672	0.6854
WI	0.9767	0.9841	0.9815	0.9809	0.9685	0.8253	0.9775	0.8037	0.9288	0.9695	0.9685
VAF	91.2618	93.9404	92.9676	92.7716	88.4684	68.3436	91.5903	89.2110	78.8948	89.2985	88.4684
NS	0.9126	0.9394	0.9297	0.9277	0.8847	0.4193	0.9159	0.1043	0.7889	0.8916	0.8847
RMSE	0.0696	0.0580	0.0624	0.0633	0.0800	0.1794	0.0683	0.2228	0.1082	0.0775	0.0800
MAE	0.0546	0.0451	0.0467	0.0480	0.0617	0.1551	0.0537	0.2098	0.0875	0.0653	0.0617
MBE	0.0000	0.0000	0.0000	0.0000	0.0000	0.1210	0.0000	0.2090	0.0002	0.0088	0.0000
RSR	0.2956	0.2462	0.2652	0.2689	0.3396	0.7620	0.2900	0.9464	0.4594	0.3293	0.3396
WMAPE	0.1301	0.1076	0.1131	0.1157	0.1469	0.3686	0.1276	0.5064	0.2077	0.1555	0.1469

Table 5 Values of performance indices of the hybrid models for the testing stage

Indices	ELM-HHO	ELM-IHHO	ELM-PSO	ELM-GA	ELM-SMA	WELM	BP-NN	SVR	RF	GMDH	MLR
R^2	0.9042	0.9254	0.9176	0.8840	0.8265	0.5467	0.8933	0.8479	0.8488	0.8468	0.8763
LMI	0.7313	0.7298	0.7110	0.6544	0.5668	0.2159	0.6563	0.1230	0.5999	0.5814	0.6330
WI	0.9748	0.9803	0.9779	0.9689	0.9523	0.8290	0.9715	0.7579	0.9393	0.9538	0.9602
VAF	90.1641	92.5374	91.7591	88.3137	82.2486	53.1123	89.2848	82.0534	82.0641	84.4496	86.8204
NS	0.9012	0.9253	0.9172	0.8827	0.8225	0.4111	0.8928	0.0474	0.8197	0.8443	0.8682
RMSE	0.0712	0.0619	0.0652	0.0776	0.0955	0.1739	0.0742	0.2212	0.0962	0.0894	0.0823
MAE	0.0482	0.0485	0.0519	0.0620	0.0777	0.1407	0.0617	0.2015	0.0718	0.0751	0.0659
MBE	0.0048	0.0013	0.0046	0.0046	0.0004	0.0785	0.0022	0.1993	0.0069	0.0028	0.0016
RSR	0.3143	0.2732	0.2878	0.3425	0.4213	0.7674	0.3275	0.9760	0.4246	0.3945	0.3631
WMAPE	0.1126	0.1132	0.1211	0.1449	0.1816	0.3286	0.1441	0.4707	0.1677	0.1755	0.1538

obtained results of the five hybrid and other employed models.

4.3 Visualisation of results

To visualise the efficiency of proposed models based on the performance parameters, graphical assessments in the form of accuracy matrix and regression error characteristics (REC) curves are presented. Note that, an accuracy matrix is a heat map matrix, recently proposed by Kardani et al. [48], which comprised various statistical parameters and is used to visualise the predictive performance of the models. Figures 10a–d and 11a–d show the accuracy matrix of all models (excluding MLR) used for predicting the permeability of tight carbonates at the training and testing stages, respectively. It may be noted that, this matrix displays the accuracy (in percentage) of performance indices in comparison to their ideal values.

Opposite to the accuracy matrix, REC curve is a modified regression version of the receiver operating characteristic (ROC) curve [76], which represents the error tolerance in the x-axis and regression precision in the y-axis. The x-axis error is typically represented by absolute deviation (AD) or

squared error (SE). However, the obtained curve presents the ‘cumulative distribution function (cdf)’ of the error. The closer the corresponding position of curve is to the top left corner, the higher is the accuracy of model.

The value of the area under the curve (AUC) can then be measured to assess the overall precision of model, preferably as large as possible, to provide an appropriate prediction. This notion of error tolerance is highly appealing since, in most regression data, the risk of inaccuracy is high due to errors and uncertainties in experiments. The REC graphs for the training and testing phases for the respective models, as well as AUC values, are shown in Figs. 12 and 13, respectively. The AUC values for all of the predictive models appear to be on the higher side. The ELM-IHHO model obtained the highest AUC value among all the other models, i.e., 0.9627 and 0.9451, during the training and testing phases, respectively.

4.4 Uncertainty analysis

In this sub-section, quantitative assessment of the developed models in predicting the permeability of tight carbonates is presented. This assessment was performed by combining



Fig. 10 a–d Accuracy matrix for the training results

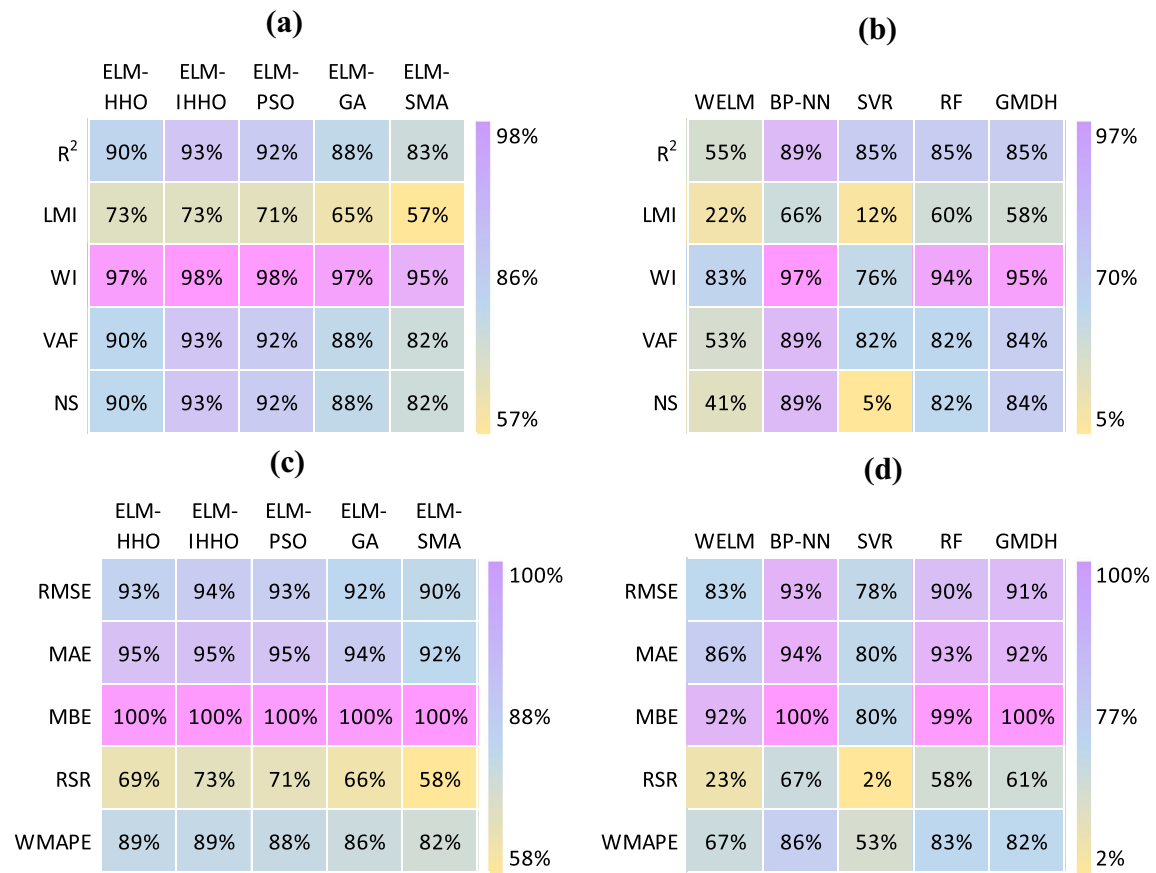


Fig. 11 a–d Accuracy matrix for the testing results

the outcomes of the training and testing datasets. The dataset includes 130 real-time observational data; hence, logical comparison of the predictive outputs can be very helpful in assessing the reliability of the predictive models. Also, the index value of the uncertainty analysis (UA) can be used to test other parameters for comparative assessment. In UA, the absolute error between the observational (y_i) and predicted (\hat{y}_i) values can be calculated as:

$$\varepsilon_i = |y_i - \hat{y}_i|. \quad (41)$$

Also, the mean of error (MOE) and standard deviation (SD) of prediction can be calculated using the following expressions:

$$MOE = \sum_{i=1}^N \varepsilon_i, \quad (42)$$

$$SD = \sqrt{\frac{\sum_{i=1}^N (\varepsilon_i - MOE)^2}{N-1}}, \quad (43)$$

where ε_i is the absolute error, and N is the number of observations; using Eqs. (42) and (43), the MOE and SD were calculated for the training and testing datasets. Afterwards, the margin of error (ME) was calculated at 95% confidence interval to determine the width of confidence bound (WCB). For this purpose, the standard error (SE), lower bound (LB), and upper bound (UB) were calculated using the following expression:

$$SE = \frac{SD}{\sqrt{N-1}}; UB = MOE + ME; LB = MOE - ME; WCB = UB - LB. \quad (44)$$

In UA, the WCB represents an error range in which approximately 95% of the whole data are located. The details of UA are presented in Table 6, indicating the values of several indices including the number of observations (N), MOE, SD, SE, ME, LB, UB, and WCB. From the index values provided in Table 6, the performance of the models can be assessed. Note that, the lower the WCB value, the greater the model certainty is, i.e., a lower WCB value indicates model has less error and can predict the desired output more accurately. Results of UA show that the ELM-IHHO model

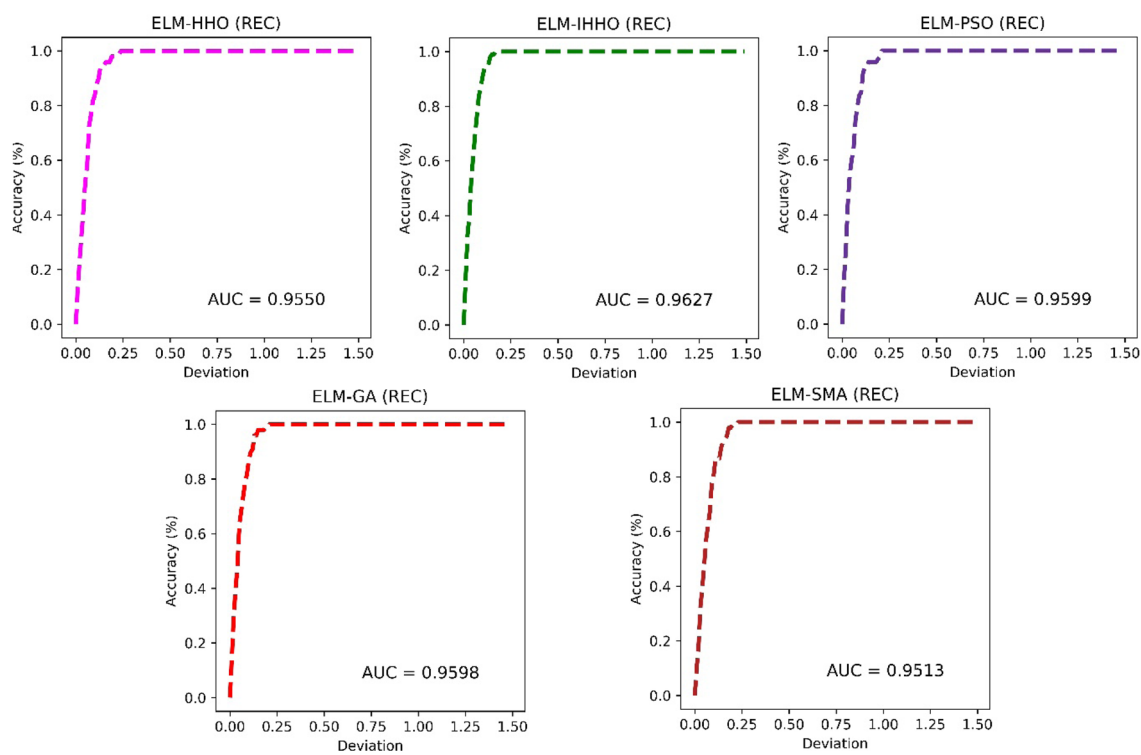


Fig. 12 REC plots of ELM-based hybrid models for the training stage

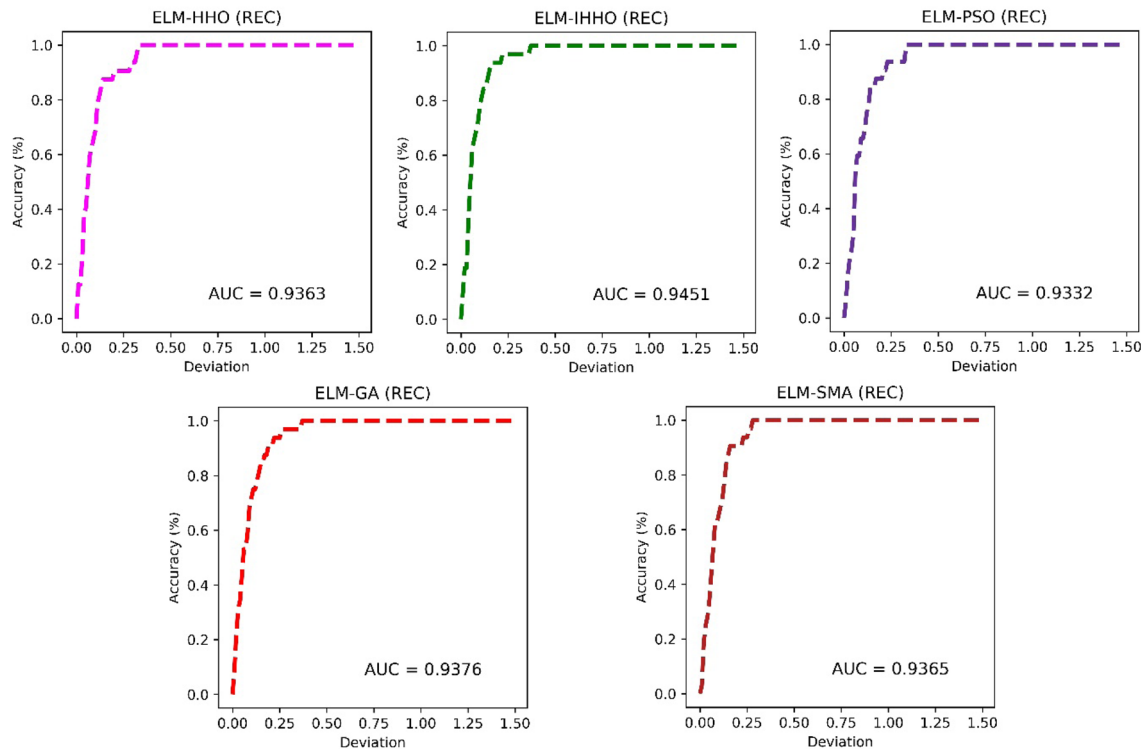


Fig. 13 REC plots of ELM-based hybrid models for the testing stage

Table 6 Results of uncertainty analysis

Model	<i>N</i>	MOE	SD	SE	ME	LB	UB	WCB
ELM-HHO	32	0.0482	0.0524	0.0093	0.0189	0.0293	0.0671	0.0378
ELM-IHHO	32	0.0485	0.0385	0.0068	0.0139	0.0346	0.0624	0.0278
ELM-PSO	32	0.0519	0.0395	0.0070	0.0142	0.0377	0.0661	0.0284
ELM-GA	32	0.0620	0.0467	0.0083	0.0168	0.0452	0.0788	0.0336
ELM-SMA	32	0.0777	0.0555	0.0098	0.0200	0.0577	0.0977	0.0400
WELM	32	0.2306	0.1256	0.0222	0.0453	0.1853	0.2759	0.0906
BP-NN	32	0.0617	0.0413	0.0073	0.0149	0.0468	0.0766	0.0298
SVR	32	0.2124	0.0827	0.0146	0.0298	0.1826	0.2422	0.0596
RF	32	0.0718	0.0641	0.0113	0.0231	0.0487	0.0949	0.0462
GMDH	32	0.0751	0.0485	0.0086	0.0175	0.0576	0.0926	0.0350
MLR	32	0.0659	0.0493	0.0087	0.0178	0.0481	0.0837	0.0356

has attained the lowest WCB and ME values of 0.0278 and 0.0139, respectively, compared to other developed models and turns out to be the most accurate predictive model. Also, the lower values of MOE, SD, and SE represent the higher reliability of the ELM-IHHO model compared to other models developed in the present study. Moreover, the WELM model with higher WCB and ME value (WCB = 0.0906 and ME = 0.0453) indicates the highest uncertainty. Therefore, the ELM-based hybrid models developed in this study, particularly ELM-IHHO, have the minimum uncertainty and highest confidence level. Graphical representation of the UA is presented in Fig. 14a–c in the form of a bar plot and line plot showing the values of SE, ME, and WCB for better comparison. Based on WCB values, ELM-IHHO is the best model followed by ELM-PSO, BP-NN, ELM-GA, GMDH, MLR, ELM-HHO, ELM-SMA, RF, SVR, and WELM.

4.5 Comparison with conventional permeability models

In this section, the obtained results from the best model amongst proposed hybrid models, i.e. ELM-IHHO, is compared to seven conventional models for predicting permeability of rocks. Table 7 shows the details of the seven conventional permeability models. While Table 8 illustrates a summary of the performance of the models in a comparative manner. As can be seen, ELM-IHHO shows the absolute superiority over the conventional models.

4.6 Discussion on results

The effects of the metaheuristic ELM-based models proposed herein were described in detail in the above subsections. In this sub-section, however, a summary overview is given. The modelling is started with developing five metaheuristic model designs based on ELM with the training dataset to display the GOF, i.e. goodness of fit, of the proposed model. In contrast, the testing dataset is employed

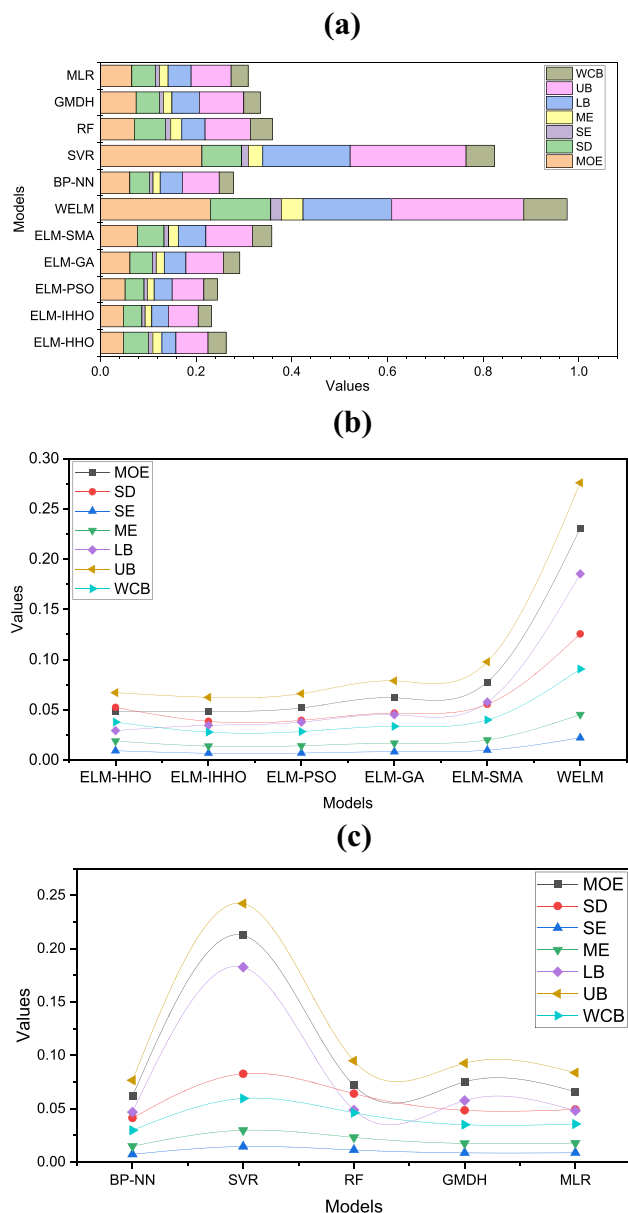
**Fig. 14** a–c Bar plot and line plot of uncertainty analysis

Table 7 Details of the seven conventional permeability models

Models	Type	Formula	Parameters
Kozeny [77] and Carmen [78]	Empirical	$\frac{cd_g^2\phi^3}{(1-\phi)^2}$	ϕ : porosity (–) d_g : mean grain size (μm) c : constant value
Berg [79]	Empirical	$8.4 \times 10^{-2} d_g^2 \phi^{5.1}$	k : permeability (m^2) d_g : mean grain size (m)
Van Baaren [80]	Empirical	$10d_d^2 \phi^{(3.64+m)} B^{-3.64}$	d_d : dominant model grain size (m) m : cementation exponent (–) B : sorting index $\begin{cases} \text{Extremly well sorted} = 0.7 \\ \text{Extremly poor sorted} = 1 \end{cases}$
RGPZ-approximate [81]	Analytical	$\frac{d_g^2 \phi^{3m}}{4am^2}$	k : permeability (m^2) d_g : mean grain size (m) m : cementation exponent (–) a : constant value (–), for spherical grain = $\frac{8}{3}$
RGPZ-exact [81]	Analytical	$\frac{d_g^2}{4am^2 F(F-1)^2}$	F : formation resistivity factor (–)
RGPZ-carbonate [25]	Analytical	$\frac{d_g^2}{4am^2 \eta F(\eta F-1)^2}$	η : multiplier for carbonate microstructure (–)
Generic [25]	Empirical	$\frac{d_g^2}{bF^3}$	b : empirically driven parameter (–)

Table 8 Performance comparison of the thermal conductivity models

Predictive models	R^2		RMSE		VAF	
	TR	TS	TR	TS	TR	TS
ELM-IHHO	0.9394	0.9254	0.0580	0.0619	93.9404	92.5374
ELM-HHO	0.9126	0.9042	0.0696	0.0712	91.2618	90.1641
ELM-PSO	0.9297	0.9176	0.0624	0.0652	92.9676	91.7591
ELM-GA	0.9277	0.8840	0.0633	0.0776	92.7716	88.3137
ELM-SMA	0.8847	0.8265	0.0633	0.0652	88.4684	82.2486
Kozeny and Carmen	0.7015	0.6621	0.0542	0.0554	70.1471	66.2132
Berg	0.6932	0.7143	0.0663	0.0663	69.3221	71.4418
Van Baaren	0.7932	0.7583	0.0538	0.0618	79.3215	75.9111
RGPZ-approximate	0.8338	0.8521	0.0410	0.0469	83.3833	85.3123
RGPZ-exact	0.8291	0.8555	0.0400	0.0428	82.9103	85.5560
RGPZ-carbonate	0.8545	0.8473	0.0943	0.0932	85.4317	84.7561
Generic	0.8697	0.8411	0.0821	0.0832	86.9452	84.1211

to validate the predictive capabilities of these models. Afterwards, the findings are analysed in depth. The measurement is initially administered using a set of performance indices. The results indicate that all models proposed in this study are able to mimic the relationships between the permeability of tights carbonates and its influential variables. In the training phase, four of the five proposed models (ELM-IHHO, ELM-PSO, ELM-GA and ELM-HHO) achieved the values of R^2 greater than 0.90. The ELM-SMA, however, achieved R^2 slightly lower than 0.90 ($R^2 = 0.8847$). Nevertheless, ELM-IHHO achieved the best predictive performance with $R^2 = 0.9394$, RMSE = 0.0580 and MAE = 0.0451, for the training dataset. For the testing dataset, ELM-IHHO achieved the best predictive performance as for the testing

dataset. However, the order of the rest four models is not similar to the one for the training dataset. ELM-IHHO is followed by ELM-GA, ELM-HHO, ELM-HHO, and ELM-SMA. Furthermore, graphical representations of the results are provided in the form of convergence curves, Taylor diagrams, accuracy matrices, and REC curves to illustrate the strength of the models proposed. The Taylor diagrams display the mathematical description of proposed models in terms of R^2 , RMSE, and variance ratios. Likewise, accuracy matrices reflect the level of accuracy (in %) achieved by the models for each performance index. Furthermore, comparative study between the conventional permeability models (i.e. analytical and empirical models) and proposed hybrid models reveals that ELM-IHHO outperforms other models.

5 Advantages, limitations and future scope of works

It may be noted that the proposed integration of ELM and IHHO shows many advantages, including very low computation cost, accelerated convergence rate, and high predictive accuracy. The proposed hybrid model achieved superior performance to the MLR model which demonstrate that, MLR technique is not always sufficient to predict the desired output for small and uncorrelated datasets. In addition, the concept of the proposed mutation-based HHO is simple and can easily be implemented. Although, the prosed concept attained a significant amount of accuracy compared to standard HHO; however, the generalisation capability can be assessed in detail in the future, which may include, implementation of the proposed concept in a more comprehensive manner by developing the improved version of other optimization algorithms and in-depth assessment using large database from different fields.

6 Conclusions

It is known that an accurate permeability calculation can save time and costs. This study proposed five hybrid metaheuristic models to predict the permeability of tight carbonates. These models were designed by combining MOAs, i.e. HHO, IHHO, PSO, GA and SMA, and ELM. ELM is used to create a mapping function that seeks to infer the value of k from various input parameters. However, MOAs are employed to optimise ELM's W&B of the linking neurons. Afterwards, it is attempted to divide the main dataset of 130 cases of tight carbonates into two subsets, namely training and testing. Here, the first and second subsets are utilised for training and validating the proposed models, respectively.

Multiple performance indices are calculated directly after the model development to test their generalisation capability and predictive accuracy. Numerical results reveal that ELM-IHHO obtained the highest predictive accuracy in both stages. All models were robust and had generalisation capability since no major changes or unacceptable values were obtained during the testing stage. Based on the outcomes, the ELM-IHHO model can be considered as a promising technique for predicting k in tight carbonates.

The purpose of this study is to replace the actual laboratory operation and include adequate details on previous AI-based studies showing their findings at all stages. Given the shortcoming, in the present study, HHO algorithm is employed to develop ELM-based HHO algorithm

(ELM-HHO). In addition, an improved version of standard HHO, IHHO, was proposed to extend local and global HHO searches by utilising the mutation-based search mechanism. The obtained results revealed that the best predictive performance in terms of computing time, convergence rate, and performance indices was achieved by the novel ELM-IHHO model. The results also suggest that the ELM-IHHO model outperforms other ELM-based metaheuristic models, i.e., ELM-HHO, ELM-PSO, ELM-GA, and ELM-SMA. The high predictive accuracy of the ELM-IHHO model suggested that it could be used as a promising tool to address real-life engineering problems. To author's best knowledge, this study pioneered using a hybrid metaheuristic optimisation model based on the ELM to predict k .

Author contributions NK: main author, conceptualisation, development of hybrid and AI models, statistical analysis, detailing, overall analysis, visualisation, original draft and manuscript finalisation; AB: development of AI and hybrid models and statistical analysis, detailing, overall analysis; BR: development of hybrid models; PS: overall review; MN: detailed review and editing; DJA: detailed review and editing; AZ: detailed review and editing.

References

1. Ma YZ, Holditch S (2015) Unconventional oil and gas resources handbook: evaluation and development. Gulf Professional Publishing, Waltham
2. Hussein D, Collier R, Lawrence J, Rashid F, Glover P, Lorinczi P et al (2017) Stratigraphic correlation and paleoenvironmental analysis of the hydrocarbon-bearing Early Miocene Euphrates and Jeribe formations in the Zagros folded-thrust belt. Arab J Geosci 10(24):543
3. Rashid F, Glover P, Lorinczi P, Hussein D, Lawrence J (2017) Microstructural controls on reservoir quality in tight oil carbonate reservoir rocks. J Pet Sci Eng 156:814–826
4. Zhang X, Spiers CJ, Peach CJ, Hebing A, Geoconsultants P (2013) Tight rock permeability measurement by pressure pulse decay and modeling. In: Proceedings of the international symposium of the Society of Core Analysts, Napa Valley, California, USA. 2013
5. Akai T, Takakuwa Y, Sato K, Wood J (2016) Pressure dependent permeability of tight rocks. In: SPE low perm symposium. Society of Petroleum Engineers; 2016
6. Al-Zainaldin S, Glover PW, Lorinczi P (2017) Synthetic fractal modelling of heterogeneous and anisotropic reservoirs for use in simulation studies: implications on their hydrocarbon recovery prediction. Transp Porous Media 116(1):181–212
7. Glover PW, Lorinczi P, Al-Zainaldin S, Al-Ramadan H, Daniel G, Sinan S (2018) Advanced fractal modelling of heterogeneous and anisotropic reservoirs. In: SPWLA 59th annual logging symposium. Society of Petrophysicists and Well-Log Analysts; 2018
8. Guo H, Zhou J, Koopialipoor M, Armaghani DJ, Tahir M (2019) Deep neural network and whale optimization algorithm to assess flyrock induced by blasting. Eng Comput 37(1):1–14
9. Duan J, Asteris PG, Nguyen H, Bui X-N, Moayedi H (2020) A novel artificial intelligence technique to predict compressive

- strength of recycled aggregate concrete using ICA-XGBoost model. *Eng Comput.* <https://doi.org/10.1007/s00366-020-01003-0>
- 10. Dhiman G (2019) ESA: a hybrid bio-inspired metaheuristic optimization approach for engineering problems. *Eng Comput.* <https://doi.org/10.1007/s00366-019-00826-w>
 - 11. Maleki E, Unal O (2020) Fatigue limit prediction and analysis of nano-structured AISI 304 steel by severe shot peening via ANN. *Eng Comput.* <https://doi.org/10.1007/s00366-020-00964-6>
 - 12. Zhu L, Zhang C, Zhang C, Wei Y, Zhou X, Cheng Y et al (2018) Prediction of total organic carbon content in shale reservoir based on a new integrated hybrid neural network and conventional well logging curves. *J Geophys Eng* 15(3):1050–1061
 - 13. Zhu L, Zhang C, Zhang C, Zhang Z, Nie X, Zhou X et al (2019) Forming a new small sample deep learning model to predict total organic carbon content by combining unsupervised learning with semisupervised learning. *Appl Soft Comput* 83:105596
 - 14. Onalo D, Adedigba S, Khan F, James LA, Butt S (2018) Data driven model for sonic well log prediction. *J Pet Sci Eng* 170:1022–1037
 - 15. Onalo D, Oloruntobi O, Adedigba S, Khan F, James L, Butt S (2019) Dynamic data driven sonic well log model for formation evaluation. *J Pet Sci Eng* 175:1049–1062
 - 16. Zhu L, Zhang C, Zhang C, Zhang Z, Zhou X, Zhu B (2019) An improved theoretical nonelectric water saturation method for organic shale reservoirs. *IEEE Access* 7:51441–51456
 - 17. Xue Y, Cheng L, Mou J, Zhao W (2014) A new fracture prediction method by combining genetic algorithm with neural network in low-permeability reservoirs. *J Pet Sci Eng* 121:159–166
 - 18. Wang H, Wu W, Chen T, Dong X, Wang G (2019) An improved neural network for TOC, S1 and S2 estimation based on conventional well logs. *J Pet Sci Eng* 176:664–678
 - 19. Lim J-S, Kim J (2004) Reservoir porosity and permeability estimation from well logs using fuzzy logic and neural networks. In: SPE Asia Pacific oil and gas conference and exhibition. Society of Petroleum Engineers; 2004
 - 20. Tang H (2008) Improved carbonate reservoir facies classification using artificial neural network method. In: Canadian international petroleum conference. Petroleum Society of Canada; 2008
 - 21. Tang H, Meddaugh WS, Toomey N (2011) Using an artificial-neural-network method to predict carbonate well log facies successfully. *SPE Reserv Eval Eng* 14(01):35–44
 - 22. Zhou X, Zhang C, Zhang Z, Zhang R, Zhu L, Zhang C (2019) A saturation evaluation method in tight gas sandstones based on diagenetic facies. *Mar Pet Geol* 107:310–325
 - 23. Zhu L, Zhang C, Wei Y, Zhou X, Huang Y, Zhang C (2017) Inversion of the permeability of a tight gas reservoir with the combination of a deep Boltzmann kernel extreme learning machine and nuclear magnetic resonance logging transverse relaxation time spectrum data. *Interpretation* 5(3):T341–T350
 - 24. Zhu L-Q, Zhang C, Wei Y, Zhang C-M (2017) Permeability prediction of the tight sandstone reservoirs using hybrid intelligent algorithm and nuclear magnetic resonance logging data. *Arab J Sci Eng* 42(4):1643–1654
 - 25. Rashid F, Glover P, Lorinczi P, Hussein D, Collier R, Lawrence J (2015) Permeability prediction in tight carbonate rocks using capillary pressure measurements. *Mar Pet Geol* 68:536–550
 - 26. Beşdok E (2004) A new method for impulsive noise suppression from highly distorted images by using Anfis. *Eng Appl Artif Intell* 17(5):519–527
 - 27. Huang J-W, Chiang C-W, Chang J-W (2018) Email security level classification of imbalanced data using artificial neural network: the real case in a world-leading enterprise. *Eng Appl Artif Intell* 75:11–21
 - 28. Janakiraman VM, Nguyen X, Assanis D (2016) An ELM based predictive control method for HCCI engines. *Eng Appl Artif Intell* 48:106–118
 - 29. Shahraiyni HT, Sodoudi S, Kerschbaumer A, Cubasch U (2015) A new structure identification scheme for ANFIS and its application for the simulation of virtual air pollution monitoring stations in urban areas. *Eng Appl Artif Intell* 41:175–182
 - 30. Singh V, Gupta I, Gupta H (2007) ANN-based estimator for distillation using Levenberg–Marquardt approach. *Eng Appl Artif Intell* 20(2):249–259
 - 31. Asteris PG, Skentou AD, Bardhan A, Samui P, Pilakoutas K (2021) Predicting concrete compressive strength using hybrid ensembling of surrogate machine learning models. *Cem Concr Res* 145:106449
 - 32. Asteris PG, Koopialipoor M, Armaghani DJ, Kotsonis EA, Lourenço PB (2021) Prediction of cement-based mortars compressive strength using machine learning techniques. *Neural Comput Appl.* <https://doi.org/10.1007/s00521-021-06004-8>
 - 33. Zhou J, Huang S, Wang M, Qiu Y (2021) Performance evaluation of hybrid GA–SVM and GWO–SVM models to predict earthquake-induced liquefaction potential of soil: a multi-dataset investigation. *Eng Comput.* <https://doi.org/10.1007/s00366-021-01418-3>
 - 34. Zeng J, Roy B, Kumar D, Mohammed AS, Armaghani DJ, Zhou J et al (2021) Proposing several hybrid PSO-extreme learning machine techniques to predict TBM performance. *Eng Comput.* <https://doi.org/10.1007/s00366-020-01225-2>
 - 35. Xie C, Nguyen H, Bui X-N, Choi Y, Zhou J, Nguyen-Trang T (2021) Predicting rock size distribution in mine blasting using various novel soft computing models based on meta-heuristics and machine learning algorithms. *Geosci Front* 12(3):101108
 - 36. Kardani N, Bardhan A, Samui P, Nazem M, Zhou A, Armaghani DJ (2021) A novel technique based on the improved firefly algorithm coupled with extreme learning machine (ELM-IFF) for predicting the thermal conductivity of soil. *Eng Comput* 1–20
 - 37. Kardani N, Zhou A, Shen S-L, Nazem M (2021) Estimating unconfined compressive strength of unsaturated cemented soils using alternative evolutionary approaches. *Transp Geotech.* <https://doi.org/10.1016/j.tgeo.2021.100591>
 - 38. R Kaloop M, Bardhan A, Kardani N, Samui P, Hu JW, Ramzy A (2021) Novel application of adaptive swarm intelligence techniques coupled with adaptive network-based fuzzy inference system in predicting photovoltaic power. *Renew Sustain Energy Rev* 148:111315. <https://doi.org/10.1016/j.rser.2021.111315>
 - 39. Bardhan A, Samui P, Ghosh K, H, Gandomi A, Bhattacharyya S (2021) ELM-based adaptive neuro swarm intelligence techniques for predicting the California bearing ratio of soils in soaked conditions. *Appl Soft Comput.* <https://doi.org/10.1016/j.asoc.2021.107595>
 - 40. Heidari AA, Mirjalili S, Faris H, Aljarah I, Mafarja M, Chen H (2019) Harris hawks optimization: algorithm and applications. *Future Gener Comput Syst* 97:849–872
 - 41. Hecht-Nielsen R (1992) Theory of the backpropagation neural network. Neural networks for perception. Elsevier, Amsterdam, pp 65–93
 - 42. Zong W, Huang G-B, Chen Y (2013) Weighted extreme learning machine for imbalance learning. *Neurocomputing* 101:229–242
 - 43. Drucker H, Burges CJ, Kaufman L, Smola A, Vapnik V (1996) Support vector regression machines. *Adv Neural Inf Process Syst* 9:155–161
 - 44. Ho TK (1995) Random decision forests. In: Proceedings of 3rd international conference on document analysis and recognition. 1. IEEE, pp 278–82

45. Ivakhnenko A, Ivakhnenko G (1995) The review of problems solvable by algorithms of the group method of data handling (GMDH). *Pattern Recognit Image Anal* 5:527–535
46. Kardani N, Zhou A, Nazem M, Shen S-L (2021) Improved prediction of slope stability using a hybrid stacking ensemble method based on finite element analysis and field data. *J Rock Mech Geotechn Eng* 13(1):188–201
47. Kardani N, Zhou A, Nazem M, Lin X (2021) Modelling of municipal solid waste gasification using an optimised ensemble soft computing model. *Fuel* 289:119903
48. Kardani N, Bardhan A, Kim D, Samui P, Zhou A (2021) Modelling the energy performance of residential buildings using advanced computational frameworks based on RVM, GMDH, ANFIS-BBO and ANFIS-IPSO. *J Build Eng* 35:102105
49. Samui P (2008) Support vector machine applied to settlement of shallow foundations on cohesionless soils. *Comput Geotech* 35(3):419–427
50. Samui P, Kumar B (2006) Artificial neural network prediction of stability numbers for two-layered slopes with associated flow rule. *Electron J Geotech Eng* 11:1–44
51. Kardani MN, Baghban A, Hamzehie ME, Baghban M (2019) Phase behavior modeling of asphaltene precipitation utilizing RBF-ANN approach. *Pet Sci Technol* 37(16):1861–1867
52. Kardani MN, Baghban A (2017) Utilization of LSSVM strategy to predict water content of sweet natural gas. *Pet Sci Technol* 35(8):761–767
53. Shang Z, He J (2015) Confidence-weighted extreme learning machine for regression problems. *Neurocomputing* 148:544–550
54. Zhou J, Qiu Y, Armaghani DJ, Zhang W, Li C, Zhu S, Tarinejad R (2021) Predicting TBM penetration rate in hard rock condition: a comparative study among six XGB-based metaheuristic techniques. *Geosci Front* 12(3):101091. <https://doi.org/10.1016/j.gsf.2020.09.020>
55. Zhou J, Qiu Y, Zhu S, Armaghani DJ, Li C, Nguyen H, Yagiz S (2021) Optimization of support vector machine through the use of metaheuristic algorithms in forecasting TBM advance rate. *Eng Appl Artif Intel* 97:104015
56. Qiu Y, Zhou J, Khandelwal M, Yang H, Yang P, Li C (2021) Performance evaluation of hybrid WOA-XGBoost, GWO-XGBoost and BO-XGBoost models to predict blast-induced ground vibration. *Eng Comput*. <https://doi.org/10.1007/s00366-021-01393-9>
57. Huang G-B, Zhou H, Ding X, Zhang R (2011) Extreme learning machine for regression and multiclass classification. *IEEE Trans Syst Man Cybern Part B (Cybern)* 42(2):513–529
58. Huang G-B, Zhu Q-Y, Siew C-K (2006) Extreme learning machine: theory and applications. *Neurocomputing* 70(1–3):489–501
59. Wolpert DH, Macready WG (1995) No free lunch theorems for search. Technical Report SFI-TR-95-02-010, Santa Fe Institute
60. Kennedy J, Eberhart R (1995) Particle swarm optimization. In: Proceedings of ICNN'95-international conference on neural networks. IEEE, vol 4, pp 1942–1948
61. Kardani MN, Baghban A, Sasanipour J, Mohammadi AH, Habibzadeh S (2018) Group contribution methods for estimating CO₂ absorption capacities of imidazolium and ammonium-based polyionic liquids. *J Clean Prod* 203:601–618
62. Kardani N, Zhou A, Nazem M, Shen S-L (2020) Estimation of bearing capacity of piles in cohesionless soil using optimised machine learning approaches. *Geotech Geol Eng* 38(2):2271–2291
63. Holland JH (1992) Genetic algorithms. *Sci Am* 267(1):44–50
64. Li S, Chen H, Wang M, Heidari AA, Mirjalili S (2020) Slime mould algorithm: a new method for stochastic optimization. *Future Gener Comput Syst* 111:300–323. <https://doi.org/10.1016/j.future.2020.03.055>
65. Koopalipoor M, Fallah A, Armaghani DJ, Azizi A, Mohamad ET (2019) Three hybrid intelligent models in estimating flyrock distance resulting from blasting. *Eng Comput* 35(1):243–256
66. Le LT, Nguyen H, Dou J, Zhou J (2019) A comparative study of PSO-ANN, GA-ANN, ICA-ANN, and ABC-ANN in estimating the heating load of buildings' energy efficiency for smart city planning. *Appl Sci* 9(13):2630
67. Roy B, Singh MP, Singh A (2019) A novel approach for rainfall-runoff modelling using a biogeography-based optimization technique. *Int J River Basin Manag* 19(1):1–14
68. Cai R, Han T, Liao W, Huang J, Li D, Kumar A et al (2020) Prediction of surface chloride concentration of marine concrete using ensemble machine learning. *Cem Concr Res* 136:106164
69. Golafshani EM, Behnood A, Arashpour M (2020) Predicting the compressive strength of normal and high-performance concretes using ANN and ANFIS hybridized with grey wolf optimizer. *Constr Build Mater* 232:117266
70. Al Khalifah H, Glover P, Lorinczi P (2020) Permeability prediction and diagenesis in tight carbonates using machine learning techniques. *Mar Pet Geol* 112:104096
71. Barton C, Woods M, Bristow C, Newall A, Westhead R, Evans DJ et al (2011) Geology of south Dorset and south-east Devon and its World Heritage Coast: special memoir for 1: 50,000 geological sheets 328 Dorchester, 341/342 West Fleet and Weymouth and 342/343 Swanage, and parts of sheets 326/340 Sidmouth, 327 Bridport, 329 Bournemouth and 339 Newton Abbot. British Geological Survey
72. Asteris PG, Mamou A, Hajihassani M, Hasanipanah M, Koopalipoor M, Le T-T et al (2021) Soft computing based closed form equations correlating L and N-type Schmidt hammer rebound numbers of rocks. *Transp Geotech*. <https://doi.org/10.1016/j.trgeo.2021.100588>
73. Kumar M, Bardhan A, Samui P, Hu JW, Kaloop RM (2021) Reliability analysis of pile foundation using soft computing techniques: a comparative study. *Processes* 9(3):486
74. Ghanbari A, Kardani MN, Moazami Goodarzi A, Janghorban Lariche M, Baghban A (2020) Neural computing approach for estimation of natural gas dew point temperature in glycol dehydration plant. *Int J Ambient Energy* 41(7):775–782
75. Ghani SK, Bardhan A (2021) A novel liquefaction study for fine-grained soil using PCA-based hybrid soft computing models. *Sādhanā* 46(3)
76. Bi J, Bennett KP (2003) Regression error characteristic curves. In: Proceedings of the 20th international conference on machine learning (ICML-03), pp 43–50
77. Kozeny J (1927) Über kapillareleitung der wasser in boden. *R Acad Sci Vienna Proc Class I* 136:271–306
78. Carman PC (1937) Fluid flow through granular beds. *Trans Inst Chem Eng* 15:150–166
79. Berg RR (1975) Capillary pressures in stratigraphic traps. *AAPG Bull* 59(6):939–956
80. Van Baaren J (1979) Quick-look permeability estimates using sidewall samples and porosity logs. In: Trans. 6th Annual European logging symposium, Society of Professional Well Log Analysts
81. Glover P, Zadiali I, Frew K (2006) Permeability prediction from MICP and NMR data using an electrokinetic approach. *Geophysics* 71(4):F49–F60

Publisher's Note Springer Nature remains neutral with regard to jurisdictional claims in published maps and institutional affiliations.